

EXPERIMENTAL CHARACTERIZATION OF BONE MATERIAL USING MICRO AND MACRO LEVEL EXPERIMENTS

A thesis submitted for the fulfilment of
Master of Philosophy at
Australian National University

By
Sudharshan Venkatesan



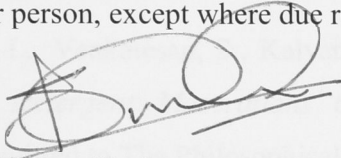
THE AUSTRALIAN NATIONAL UNIVERSITY

August 2008

Declaration

Journal Papers

This is a declaration that this thesis contains no material that has been accepted for any other degree or diploma in any other university. To the best of the author's knowledge and belief, it contains no material previously published or written by any other person, except where due reference is made.



Sudharshan Venkatesan

Yiu, L., Venkatesan, S., Kalymoncherry, S., Qin, Q., Effect of Micro-structure on Macro-mechanical performance of Dry Cortical Bone tissue. (Submitted to Acta Biomaterialia, 2009)

Yiu, L., Venkatesan, S., Kalymoncherry, S., Qin, Q., Effect of Dry-Substituted micro-structure on the mechanical properties of Hydrated Cortical Bone tissue.(Article in draft)

Conferences/Papers

Venkatesan, S., Yiu, L., Kalymoncherry, S., Qin, Q., A study of real time strain measurement system for analysis of Strain Evolution and Failure behaviour of Cortical Bone-tissue. Second Asia Pacific Workshop on Structural Health Monitoring, Melbourne, December 2008

Publications from this research

Journal Papers

Venkatesan, S., Yin, L., Kalyanasundaram, S., Qin, Q., *Micro indentation Behaviour of Hydrated and Dehydrated Compact bones using Confocal Laser Microscopy (article in draft)*

Yin, L., Venkatesan, S., Kalyanasundaram, S., Qin, Q., *Influence of Water, Trypsin and Detergent Macerations on Micro-structure and Micro-hardness of bone.* (Submitted to The Philosophical Magazine, 2008)

Yin, L., Venkatesan, S., Kalyanasundaram, S., Qin, Q., *Effect of Micro-structure on Micromechanical performance of Dry Cortical bone tissues.* (Submitted to Acta Biomaterialia, 2008)

Yin, L., Venkatesan, S., Kalyanasundaram, S., Qin, Q., *Effect of Cryo-induced micro cracks on the mechanical properties of Hydrated Cortical bone tissue.*(Article in draft)

Conference Papers

Venkatesan, S., Yin, L., Kalyanasundaram, S., Qin, Q., *A study of real time strain measurement system for analysis of Strain Evolution and failure behaviour of Cortical Bone Material., Second Asia Pacific Workshop on Structural Health Monitoring, Melbourne, December 2008*

Acknowledgements

I would like to thank my supervisors, Dr. Shankar Kalyanasundaram, Prof. Qinghua Qin and Dr. Ling Yin, firstly for having given me an opportunity to undertake this research project and secondly for their excellent guidance, support and advice throughout the duration of this study. Dr. Shankar especially for the encouragement and the opportunities provided and for being a friend with whom I could discuss issues other than those pertaining to the study, Prof. Qinghua Qin for the support both academic and financial and Dr. Ling Yin for the expert advise on experimental procedures and the insight into the microstructural behaviour of bones. I would also like to extend my thanks to Dr. Zbigniew Stachurski and Mr. Tony Flynn for their extended support through the course of my study. I would like to thank the technical staff for their support and guidance. I would also like to thank Mr. Daryl Webb for guidance and valuable discussions at the Electron Microscopy Unit. I have also found a good friend in Sivakumar to whom I extend my gratitude for being a major source of moral support. Above all I would like to thank my parents without whose support and encouragement none of these would have ever been possible.

Contents

Abstract

Introduction

Background and Research

In the past few decades, extensive studies have been carried out to understand the mechanical properties of the bone. The mechanical properties and failure of the bone give insight into bone healing process and this in turn is important to the treatment of bone and bone related diseases. Whilst significant advances have been made in the bone remodelling, an understanding of the evolution of strain during mechanical loading and the effect of this strain evolution to fracture of bone materials is yet to be developed. This study aims to understand the mechanical performance of the cortical bone at the micro and the macro scale. At the micro scale experiments have been conducted to understand the mechanical properties by the calculation of the hardness of bone and its variations with governing factors and at the macro scale, an extensive study of the mechanical properties was conducted by the study of real time strain evolution. Real time strain measurements have been performed at the macro level during compression and 3 point bend testing. There have been significant effects of sample size and loading rate observed during compression testing. The test results elucidate viscoelastic properties of compact bone during real time testing. Rate dependant failure behaviour has been observed during the bending tests. An increase in the loading rates has shown a significant increase in the strain values measured. Two notable different failure mechanisms were observed during the bend testing.

Removal of soft tissue

Preparation of test sections

3.2.1 Micro-structural analysis and porosity measurement

3.2.2 Hardness measurement of bone

3.3 Results

3.3.1 Removal of soft tissue

3.3.2 Hardness

3.3.3 Microhardness

3.4 Discussion

3.5 Conclusion

4. Mineralization of cortical bone

Contents	43
3.2. Experimental procedure	44
Declaration	ii
Publication from this Research	iii
Acknowledgments	iv
Abstract	v
Table of contents	vi
List of figures	ix
List of tables	xii
1. Introduction	1
2. Literature review	6
2.1. Bone , Structure and Hierarchy	6
2.2. Micro-mechanical properties	10
2.3. Material properties	16
2.4. Failure mechanisms	20
2.5. Current study	25
3. Sample preparation	27
3.1. Introduction	28
3.2. Experimental procedure	29
3.2.1. Removal of soft tissue	29
3.2.2. Preparation of thin sections	30
3.2.3. Microstructural analysis and porosity measurement	31
3.2.4. Standard microindentation testing	32
3.3. Results	33
3.3.1. Removal of soft tissue	33
3.3.2. Microstructure	34
3.3.3. Microhardness	38
3.4. Discussion	39
3.5. Conclusions	42
4. Microindentation of cortical bone	43

4.1. Introduction	43
4.2. Experimental procedure	44
4.2.1. Sample preparation	44
4.2.2. Microindentation of wet and Dry Compact Bone	45
4.3. Results	46
4.3.1. Micromechanical performance analysis	46
4.3.2. Effect of physiological condition	53
4.4. Discussion	56
4.5. Conclusion	59
5. Real time strain measurement during compression	61
5.1. Introduction	61
5.2. Sample preparation	62
5.3. Compression testing	63
5.3.1. Mechanical apparatus	63
5.3.2. Control system	63
5.3.3. Compression test procedure	64
5.3.4. 3D real time strain measurement	65
5.3.5. Specimen Preparation	68
5.4. Compression testing of specimen	69
5.5. Results and Discussions	69
5.5.1. Load – Displacement data	69
5.5.2. Strain Distribution	72
5.5.3. Effect of Sample Size	77
5.5.4. Effect of Strain Rate	77
5.6. Microscopic Observations	78
5.6.1. Failure Behaviour	78
5.6.2. Rate Dependency	81
5.7. Conclusions	83
6. 3 Point Bend Testing of Compact Bones	84
6.1. Introduction	84
6.2. Experimental Procedure	85
6.2.1. Sample Preparation	85

6.3. 3 Point Bend Test Procedure	85
6.3.1. Mechanical Apparatus	85
6.3.2. 3 Point Bend test Procedure	86
6.3.3. 3D Real Time Strain Measurement	87
6.4. 3 Point Bend Testing	87
6.5. Results and Discussion	88
6.5.1. Load Displacement Data	88
6.5.2. Failure Behaviour and Strain Distribution	90
6.5.3. Effect of Strain Rates	97
6.6. Conclusion	99

7. Conclusions

References

Appendix A – Load Displacement Behavior

Appendix B – Von Mises strain distribution

List of Figures

Figure 3.1.	Scanning electron micrographs of microstructures of the bones macerated in (a) Solution A (water only), (b) Solution B (with trypsin), (c) Solution C (with Surf) and (d) Solution D (with Biozet).	36
Figure 3.2.	High-magnification microstructure of the compact bone.	37
Figure 3.3	High-magnification of woven and lamellar structures.	38
Figure 3.4.	Porosity identification and distribution of pore diameters.	38
Figure 3.5.	Porosity of bone macerated in each solution	40
Figure 3.6.	Vickers hardness for the bones macerated in the different solutions.	41
Figure 4.1.	Vickers hardness of dry bone (lamb femurs).	48
Figure 4.2.	BSE images of the indentation patterns at loads	49
Figure 4.3.	Recovered Vickers hardness measured under SEM in comparison with the initial measurements	50
Figure 4.4.	High-magnification BSE images of the indentation patters at the applied load of 9.8 N.	51
Figure 4.5.	High-magnification BSE images of the indentation patterns at the applied load of 4.9 N.	52
Figure 4.6.	High-magnification BSE images of two indentation patterns at the applied load of 1.96 N.	53
Figure 4.7.	High-magnification BSE image of the indentation pattern at the applied load of 0.45 N.	54
Figure 4.8.	High-magnification BSE image of the indentation pattern at the applied load of 0.245 N.	54

Figure 4.9.	Vickers hardness of dry bone and wet bone versus the indentation force (lamb femurs)	55
Figure 4.10.	Confocal laser scanned images of the indentation patterns at various depths in a dry cortical bone sample	56
Figure 4.11.	Confocal laser scanned images of the indentation patterns at various depths in a wet cortical bone sample	57
Figure 4.12.	High-magnification image of an indentation pattern.	58
Figure 5.1	Experimental set up for compression testing	66
Figure 5.2	A typical stochastic pattern on bone sample	69
Figure 5.3	Load Displacement Curve for bone sample of length 30mm tested at a strain rate of 1.3mm/min.	69
Figure 5.4	Load Displacement Curve for bone sample of length 50mm tested at a strain rate of 1.3mm/min	70
Figure 5.5	Load Displacement Curve for bone sample of length 30mm tested at a strain rate of 3.3mm/min.	70
Figure 5.6	Load Displacement Curve for bone sample of length 50mm tested at a strain rate of 3.3mm/min	71
Figure 5.7	Von Mises strain distributions in bone samples tested at 1.3mm/min	72
Figure 5.8	Von Mises strain distributions in bone samples tested at 3.3mm/min	73
Figure 5.9	Major strain distribution in samples tested at a strain rate of 1.3 mm/min	75
Figure 5.10	Major strain distribution in samples tested at a strain rate of 3.3 mm/min	76
Figure 5.11	Magnified images of bone fracture.	79
Figure 5.12	Fracture in the cross section of bone	80
Figure 6.1	Load Displacement curve for bone in 3 point bending for sample tested at a strain rate of 1.3 mm/min	88

Figure 6.2	Load Displacement curves for samples tested at different loading rates	88
Figure 6.3	Von Mises strain distribution in sample loaded at a rate of 1.3 mm/min.	90
Figure 6.4	Von Mises strain distribution in sample loaded at a rate of 2.3 mm/min	91
Figure 6.5	Von Mises strain distribution in sample loaded at a rate of 3.3 mm/min	91
Figure 6.6	Typical damage in sample loaded at 1.3 mm/min	92
Figure 6.7	Major strain distribution in sample loaded at 1.3 mm/min during the test	92
Figure 6.8	Typical damage in sample loaded at 2.3 mm/min	93
Figure 6.9	Major strain distribution in sample loaded at 2.3 mm/min during the test	93
Figure 6.10	Typical damage in sample tested at 3.3 mm/min	95
Figure 6.11	Major strain distribution in sample loaded at 2.3 mm/min during the test	95
Figure 6.12	Microscopic observations of the failures	96

List of Tables

Table 3.1	pH value of test solutions	29
Table 3.2	Standard microhardness indentation tests	38
Table 5.1	ARAMIS system specifications	66

Chapter 1

INTRODUCTION

Bone is an important structural component of the body which is designed to contain load bearing capabilities. It is a complex ceramic of hydroxyapatite. The structure of the bone plays an important role in the capabilities of the bone. As a biological material, the bone is composed of regenerative cells, blood vessels and a mineralized extra-cellular matrix of calcium and hydroxyapatite. The mineral crystals are embedded in collagen fibers through the bone. The micro structure of the bone is classified into two categories based on the architecture at the region; cortical bone, with a compact mineralized connective tissue with very low porosity, and trabecular bone with lesser connective tissue and architecture with very high porosity. Further more, bone consists of woven lamellar layers. Woven bone is weak, with a small number of randomly oriented collagen fibers, but forms quickly without a preexisting architecture during bone repair or growth. Lamellar bone is stronger, consisting of numerous stacked layers and is filled with many collagen fibers parallel to other fibers providing strength to the bone.

It has been shown that the mechanical properties of the bone vary in different regions in the bone. This has mainly been attributed to the architecture of the bone microstructure. Cortical bone is known to be stronger than trabecular bone.

The study of bones with an aim to characterize the material has been pursued over decades and is discussed in Chapter 2. There has been extensive work done at different levels: nano scale, micro scale, macro scale. Through the course of these extensive studies, bone has been subjected to various mechanical loading conditions. Although investigators have produced results that show the strength of bone, there is little knowledge of real time strain evolution patterns during the mechanical testing of bone.

The rationale for this project stems from an effort to characterize lamb femurs under various types of mechanical loading conditions. The study also focuses on characterizing strain evolution patterns in cortical bone during mechanical testing of bone samples.

Though characterization of bone samples have been carried out for decades, they have inclined towards medical treatment. The mechanics of bone studies can be best described by Voigt's model, Reuss model and the Katz equation [1]. Although these models form good limiting conditions for bone testing, they fail to completely explain the failure behavior of bones.

This is the motivation for this research project, which aims to understand and provide a novel experimental study by studying the failure of bones at micro and macro levels and by the analysis of real time strain evolution during mechanical loading of bones.

Research Aim

To characterize cortical bones obtained from lamb femurs under different mechanical loading conditions.

Whole bones consist of mainly three different types of material; the cortical bone, the trabecular bone and the bone marrow along with biological cells and blood and fluid vessels. The cleaning of fresh bones to remove these soft tissues while maintaining their structural integrity is a basic and essential part of bone studies. The primary issues include how the cleaning should be efficiently and safely conducted and how the process itself influences bone microstructure and mechanical properties of bone samples prepared using these methods. Scanning electron microscopy was used to compare the microstructure of the samples prepared. The porosity of the samples was quantified using image processing software. Microhardness of the bones was measured using a Vicker's indentation tester for the verification of the mechanical properties of the samples prepared using different techniques. The results of these studies are presented and discussed in detail.

With the knowledge of bones having a hierarchical architecture, this study has been focused on determining mechanical properties of bones in both the micro and the macro levels. At the micro level, micro hardness was chosen as an effective measure of the mechanical properties of the cortical bone. Chapter 4 deals with the use of micro indentation techniques to measure the micro hardness of the compact bone samples derived from lamb femurs. The detailed sample preparation techniques and the results of the microindentation tests have been elucidated.

The study also describes the effect of the physiological condition of the bone samples and relates the changes of that condition to changes in the micro

hardness of the bone samples prepared. To better understand the indentation behavior, different magnification techniques such as Scanning Electron Microscopy and Confocal Laser Scanning Microscopy have been used. The images obtained through these techniques highlight the mechanical properties and dependence of these mechanical properties on the microstructure and the architecture of the bone material.

Furthermore, damage has been induced in bone samples using a quick freeze technique by creating cracks with the order of lengths in the micro scale. Changes in the mechanical properties of the bone samples have also been described in Chapter 3.

The macro level experiments that have been performed during the course of this research project are in the form of compression and three point bend testing on lamb femurs. The tests have been designed to elucidate key mechanical properties of bone material. A real time strain measurement system in the form of the ARAMIS 3D Photogrammetry system was used to elucidate the failure behavior of bones. Bones are designed to have certain load bearing capabilities with the longitudinal axis designed to bear loads in compression and bending loads during trauma of an accident, extreme activities and day to day activities at lower loads. Standard mechanical tests have been used over the decades to study mechanical properties of bone. These standard test methods only deliver integral information of the bone but do not provide any information about the processes during testing. Thus experiments were designed to understand the strain evolution during testing better. Chapters 5 and 6 offer, in depth, the processes of the testing in compression and 3 Point Bend testing.

Surface strain was calculated using high speed photographs of the bone during testing. Using these images strain was calculated and the evolution of failure was determined. The surface strain in bones is an important aspect to be considered as it described the failure behavior and fracture evolution at the interface of the bone and muscular system. The observations contained in Chapters 5 and 6 provide a clear picture of the local processes used during testing and thus give a new perspective to failure behavior and strain evolution in bones through a novel experimental procedure.

- * 10% collagen
- * 40% mineral
- * 50% water

* Woven bone

Woven bone is laid down very quickly and mainly arranged during fracture development and fracture repair. The bone fibers are randomly oriented randomly. Woven bone also contains 90% water in the lamellae and osteoclasts and blood vessels.

* Lamellar bone

In lamellar bone the collagen fibers form bundles of 2-3 μm bundles which are arranged parallel to each other. The orientation of fibers and collagen bundles are laid down as lamellae

Chapter 2

LITERATURE REVIEW

2.1 Bone: Structure and Hierarchy

Weiner and Wagner refer the term bone to a family of materials which have basic building blocks in the form of mineralized collagen [2]. Bone consists of fibrous collagen embedded in a mineral matrix of calcium phosphate. Considering that a further main component of bone is water, the average composition of a healthy mammalian bone is:

- 10% collagen
- 65% minerals
- 25% water

On the basis of structural differences on a microscopic level, mammalian bone can be classified into three different groups:

- Woven bone

Woven bone is laid down very quickly and mainly emerges during fracture development and fracture repair. The fine fibred collagen is oriented randomly. Woven bone also contains cells such as the osteoblasts and osteoclasts and blood vessels.

- Lamellar bone

In lamellar bone the collagen fibers form bundles of 2-3 μ m lamellae which are arranged much more precisely than in woven bone. The orientation of fibers and correlated minerals are laid down as lamellar

with thickness of about $1\mu\text{m}$ [1]. Lamellar bone shows a slightly lower mineral content than woven bone.

- Parallel fibred bone

Parallel fibred bone can be seen as an intermediate between woven and lamellar bone. It has a high mineral content but the collagen fibers are not totally randomly oriented as they are in woven bone. This form of bone can be found in specific situations according to the function of the bone.

Weiner and Wagner [2] also equate the bone to man made composites where structure and properties show progressively less anisotropy. This phenomenon is explained by the arrangement of lamellae in layered or laminated structures. This design of the structure in bones makes it capable of load bearing and a variety of stress handling capabilities in various directions. At the macro level, bone can be classified into two types with different visible mechanical properties. The main structures can be distinguished as

- Compact Bone

Compact bone, also called cortical bone, is almost completely solid. Small spaces are filled mainly by living cells and blood vessels. The shafts of long bones are made of compact bone. These bones are cylindrical in shape and are filled with bone marrow.

- Cancellous Bone

Cancellous bone, also called trabecular bone, has a porous structure. Cancellous bone has a higher anisotropic property than that of compact bone. Normally, cancellous bone is located inside compact bones at

points or regions with high loads to support the outer shell. Typically, such areas are the ends of weight bearing long bones. Adult cancellous bone is usually made of lamellar bone.

The study of the micro-structure of the bone has been the subject of several investigations over the last few decades. Cedola *et al* [3] studied the interaction of new formed mineral crystals and the scaffolding fibers that led to the imposing of a desired 3 dimensional architecture in bones during growth process. A small angle X ray scattering technique was used by Cedola and his colleagues using synchrotron radiation. Microscopic maps of the degree of mineralization, the presence of collagen and the mineral orientation degrees were obtained using this novel technique. They have also indicated the correlation of these three factors as the mineralization degree representing the bone growth process and the use of the distribution of mineralization. The interaction between the newly deposited bone and collagen scaffolds is known as a key factor in the structural properties of bones.

The mineralization of bone has also been characterized by D A Bradley [4] using X ray fluorescence microscopy available from synchrotron radiation. The main study was performed on trabecular bone to determine the distribution of minerals and their differential location at the bone- cartilage interface and the surface of the trabeculae. These are related to the bone remodeling process through this study. The study of bone structure and composition has also been pursued using synchrotron radiation by many research groups [5-8]. The other methodologies that have been used are the Auger Electron spectroscopy [9], micro CT analysis [10] and Ultrasonic technologies [11].

Chaffai *et al* [11] determined the relationship between ultrasonic backscatter, density and micro- architecture of cancellous bone. In their study, X- ray quantitative computer tomography was used to determine Bone Mineral Density (BMD) and synchrotron radiation microtomography technique was used to investigate the bone microarchitecture. The investigation assessed the variables of the ultrasonic technique and their association with the density and micro- architecture using simple and multi- variate linear regression. This study highlights unaccounted variance in parameters whose source remains unknown emphasizing further need for investigation.

The study of bone structure and architecture along with bone remodeling has interested both clinical and engineering fields. The investigation of the clinical implications of these factors is based on the understanding that it would lead to better knowledge of bones' ability to resist fracture. This information could be used to identify new therapeutic intervention and to develop better biomarkers and noninvasive modalities. Mary L Bouxsein [12] stresses that despite the current usage of the BMD technique as a diagnostic tool to monitor bones, there could be the possibility of opening new arenas that could help design therapeutic interventions that could lead us to help prevent fractures and maintain bone health.

Biomedical engineers have also pursued bone studies with emphasis on the structure and architecture of bone material. Efforts have been made to develop natural hydroxyapatite, which is an essential component of the bone material that could be used on reconstructive orthopedics and other surgery procedures. Composite materials have also been developed using

hydroxyapatite that could be molded into different shapes which could be used in bone repair, bone graft and other clinical processes [13]. These studies are focused on the objective of producing an ideal biomaterial.

Tissue engineering also highlights the need to further enhance our knowledge of the interactions of the growth factors with other cells and with each other, their efforts and the methods of triggering intercellular pathways. These investigations aim to increase our understanding of the processes of activating and deactivating the interactions between growth factors and other cells during the bone growth and bone remodeling process. Tissue engineering stresses the need for the enhanced understanding of materials behavior in order to design and develop newer and more effective biomaterials [14].

2.2 Micromechanical properties

The need to first understand the materials characteristics has been brought forth time and again. The need to gain insight into fracture mechanisms of bone is essential for contributions to the clinical management of fracture, the technology of orthopedic intervention and the understanding of the physiology of bone tissue regeneration and healing. The characteristics of bone tissue are raised including the brittle nature, anisotropy, viscoelastic properties, hardness, deterioration with age and the ability to heal. The study of these characteristics has been pursued since the use of microindentation in the 1920s. Micro-indentation has been used to investigate the variation of bone hardness and anisotropic nature of bone. Microindentation is the action of forming an impression on the surface at a micro level.

Most previous biomechanical tests on bone have focused on macroscopic fracture based on structural characterization [15]. The outcomes lack the visualization of submicroscopic damage [15]. As a biological material, bone exhibits a complex microstructure and microcomponents, which result in complicated mechanical properties [16-22]. Recently, these properties have begun to be addressed quantitatively with regard to the microstructure of the tissue [16]. Microscopic damage in bone was found to contribute in a significant manner to an increase in bone fragility, leading to complications such as osteoporotic and stress fractures [15]. Microcracks can affect the mechanical properties of bone, giving rise to a decrease in strength and stiffness, and a decrease in fracture resistance. The accumulation of such damage may occur due to normal daily activities. For example, several studies have related fatigue or cyclic loading to microcrack formation [15, 22, and 24]. Cortical bone has a strongly hierarchical structure, in which there are phase and material direction changes over many length scales and a porosity of about 5% due to the presence of blood vessels and living cells [24]. These heterogeneities account for the ability of bones to contain stable cracks that can vary greatly in length. It is very difficult to determine at what level the processes leading to failure occur due to the complicated interactions between heterogeneities and microcracks when considering failure behavior. The effects of the microstructure of bone on crack propagation and mechanical properties need to be investigated [16].

Indentation tests represent a promising direction in characterizing the quality of bone repair as a function of location [15, 22–28]. These tests have been used to measure local mechanical properties of callus and the surrounding

tissues. Hardness is the resistance of a material against deformation under indentation by an object. The advantage of hardness tests is that these tests can be done on very small specimens [15]. Microhardness is measured from the penetration of an indenter, which makes imprints of microscopic size, thus allowing the determination of hardness in small areas of the sample. Previous studies using microindentation mainly focused on microhardness anisotropy of compact bone [27–32] and hardness measurement of human enamel and dentine material [33, 34].

Microindentation offers a means of characterizing the deformation properties of bone and provides a basis for evaluating a range of contact-related properties, particularly surface-damage phenomena in sharp-particle compression [34]. Furthermore, imaging of micro-indented patterns using scanning electron microscopy can provide insight into the material response to mechanical loads at the micro scale to identify the role of microstructure of bone in damage. The hardness is known to be higher in samples from either the dehydrated or embedded tests. Microindentation patterns are also clearer in dry or embedded conditions than those on the wet samples. It has also been known that dry or embedded conditions are not ideal and the wet condition would be closer to the one *in vivo*.

Microhardness of the bone is also known to vary with five independent variables. The variables have been named by Johnson et al. [35] as applied mass, dwell time, drying time between indentation and measurement and the distance between the centre of an indentation and the edge of other indentations and pores. The minimum applied mass of 0.1 kg is prescribed in order to get

reproducible results for bovine bones. The dwell time was found to have no significant effect on the hardness of bones. The derived hardness too had no significant changes with the removal of samples from the solutions for up to 1.75 hours. The times between indentation and measurement were found to have changes in the measured hardness. But there have been studies showing a viscoelastic recovery after microindentation for the first 24 hours. The distance between the indentation and the pores plays an important role in the hardness calculated. It is now shown by Johnson et al. that there is a significant change in the hardness calculated if the indentation were to be within a distance of $70\mu\text{m}$ from the pores. There has been a significant interaction between the applied mass and dwell time but has shown to be limited to lower loads of 0.01kg. [35]

The deterioration of bone material with age and the mechanical characteristics have been the subject of immense interest. Zioupos [36] studied the variation of toughness of ageing bone with age and has also examined the fracture profile morphology by the use of fractal analysis. It has been shown that the fracture of bones in either a slow or fast fashion has a connection with architectural status and the changes in bone with age. In this investigation, Zioupos has studied the work of fracture in bone samples. It was seen that a crack had started when micro cracking toughening was the dominant phenomenon. These parent cracks could be affected by crack deflection and could be influenced by crack bridging forces. These observations were related to ambient conditions and the microstructure of bones.

The fracture of bone is also known to be dependant on the components of the bone. The role of collagen and other organic material present in the bone

tissue are best described by Currey [37]. He has found that the collagen when damaged, results in a lowered toughness and strength but did not change the stiffness. A polymorphism associating the role of collagen and bone diseases like osteoporosis was highlighted as well. The research also adds that the changes in the collagen properties may alter the amount of mineralization which would affect the bone mechanics, even if the collagen were to remain undamaged. It is now known that the interaction of fibers and the matrix are very different from that of man-made composites to bones. [37]

The other main characteristic of bone material is its anisotropic nature. Won-Jin Yi et. Al [38] has successfully shown that a direct measurement of the anisotropy in bones is possible by the use of fractal dimension and the principal axes of inertia. The anisotropy was measured using radiographs from human mandibles based on the principal axes and best fitting ellipse. It was found that the anisotropy was higher in the incisor region of the mandibles than that at the angle region. Anisotropy has also been clearly documented by Evans et al [24]. The bone is known to be stronger in the longitudinal direction. Also, bone material is stronger in compression than in tension. The compressional behavior is characterized by some softening after the elastic region is reached. This is mainly due to the formation of shear planes at the structural level. These shear zones are a result of the localized buckling of the collagen fibrils. It is also known that the angle of the buckling region to the loading axis varies from 30 - 40°. These are the adaptations of nature as the strength of the bone is required in the longitudinal direction and the bone in real life is never loaded radially.

The anisotropy in the viscoelastic properties is also conceded as an important aspect of the cortical bones. Toshiya Iyo et al [39] have determined the effect of anisotropy on the relaxation modulus of cortical bone. The transmission of the force along the longer axis in bone was found to be due to the effect of the collagen present. Increase to the reinforced collagen matrix is known to be the cause of the longer relaxation time with increase in the mineral fraction.

Viscoelastic behavior is shown by a strong effect of the strain rates applied during the mechanical testing of bones. The failure of cancellous bone and the viscoelastic effect has been well described by R. M. Guedes et al [40]. It has been shown that a linear correlation between the collapse stress and the Young's modulus exists. Viscoelasticity has also been found in the recovery of the impressions created by microindentation in bone samples. The impressions were found to recover by over 50% in the 24 hours immediately after the tests.

The damage mechanisms in bone material have also been of great interest over the last few decades. The damage modes are different during different methods of testing. The failure in tension is known to be mainly due to the opening of bone wherein the crack propagation was found to be propagating in a direction perpendicular to the test axis. In contrast to tensile failure, failure in compression is known to be mainly due the in-plane shear resulting from the test. Torsional failure is known to be a combination of these two modes of failure. Damage development in cortical bone therefore is dependant on the mode of loading. [41, 42]

The highly heterogeneous structure of bone has been known to play an important role in the failure of bones. The effect of this heterogeneous nature is

depicted by the effect of the rate of loading during the testing of bones. The fact that at high strain rates bone elastic modulus decreases and ultimate strength increases suggests that the design of bone is naturally adapted for its dynamic mechanical function. [43]. Ferreira [44] has confirmed through his research that bone is very heterogeneous and this is shown by the significant scattering of results. He has also showed that an increase in the strain rate leads to an increase in the resistance properties and a decrease in the stiffness of the bone. The scattering of the results in this study have been partially attributed to the complex nature of the microarchitecture of the bone material. Light has also been thrown on the need for further study on the effects of defects, sample size and stress propagation through the structure of the bone.

2.3 Material Properties

The architecture of the bone has also been of great interest as it is a very important factor governing the strength of the bones. It has been shown that the variation in the architecture of the bone shows direct variations in the mechanical properties thereby highlighting the dependence of the mechanical properties on the microarchitecture of the bones. In osteoporotic conditions, the microarchitecture of the bone is known to undergo drastic changes. The deterioration during this condition is characterized by an abnormal porous structure with an increase in the porous nature with the varied stages of this condition. Studies of the dependence of the mechanical properties on the architecture of the bone have resulted in many important findings. Topological parameters such as lacunarity have been used to determine the strength of bones.

Tools such as the lacunarity have now been proposed for usage in the detection of various stages of osteoporosis. [45].

The modeling of Young's modulus has seen several attempts over the years of bone studies. Young's modulus of cortical bone is known to have a variation between 8 – 24 GPa. This value for bone is much lower than that of hydroxyapatite which is known to have a modulus of approximately 130 GPa. Collagen is not linearly elastic, but the use of a tangent modulus can define the value for the material at about 1.25 GPa. Based on the knowledge of composites attempts for the modeling of these characteristics of bone have been shown by Voigt's model and the Reuss model. These form the limiting conditions during the testing of bone based on the direction of the load application. The Voigt model is described by the equation

$$E_b = V_{ha} E_{ha} + V_c E_c$$

This model describes the Young's modulus when the loading is in the direction of the orientation.

Reuss model is described by the equation

$$\frac{1}{E_b} = \frac{V_{ha}}{E_{ha}} + \frac{V_c}{E_c}$$

Where, E_b = Young's Modulus of Bone

E_c = Young's Modulus of Collagen

E_{ha} = Young's Modulus of Hydroxyapatite

V_b , V_c and V_{ha} are the Volumes of Bone, Collagen and Hydroxyapatite respectively.

This model describes the Young's modulus when the loading is perpendicular to the direction of orientation.

Although these models take into account the hydroxyapatite content and collagen, they provide a wide range of value for the Young's modulus which is unacceptable. Experimental results from the literature have shown the Young's modulus of most animal bones to be within these values thereby calling these models as limiting conditions [46, 47]. The Young's modulus is by far best described by Katz equation, which is essentially a Voigt's model. He does take into account the orientation of collagen fibrils, each having a fraction f_i and an angle φ_i with the loading axis. Katz equation calculates Young's modulus as

$$E_b = \frac{E_c V_c (1 - \nu_c \nu_b)}{1 - \nu_c^2} + \sum E_{ha} V_{ha} f_i (\cos^4 \Phi_i - \nu_b \cos^2 \Phi_i \sin^2 \Phi_i)$$

The toughness of bone is another important factor that influences the failure behavior of bone materials. A study of leg bones by Gibeling *et al* [48] has shown that fracture toughness increases with crack length. This increase in fracture toughness with crack growth indicates mechanisms of toughening of the material are a result of the ceramic matrix and the presence of minerals. A decrease in stress concentration can also be attributed to microcrack development in the ceramic matrix. Other methods like the R curve have been used to determine fracture toughness as it is dependant on the crack growth. These studies have revealed debonding mechanisms to be occurring ahead of the crack propagation. This debonding could result in the crack energy absorption, crack deflection and toughening.[34] Crack bridging is also a phenomenon observed by Ritchie *et al*, phenomenon where cracks occur in zones of damage and are not connected to each other. This results in bridges forming between the cracks as crack grows. [27]. Nalla *et. al* [49] have also highlighted the importance of localized fracture criteria and toughening mechanisms to the fracture in human

bones. The mechanism of microcracks has been widely investigated in the fracture of metals and ceramic materials but has not been well extended into bone and other biological materials. [49]. With the use of a Double Notched four point bend test, Nalla *et al* shed light on localized cracking events that lead to catastrophic failure and toughening mechanisms in bone. Their research has confirmed that the onset of failure in bones is consistent with a strain based criteria as used in many finite element models. Nalla has also provided evidence that toughening arises from a number of sources like crack bridging between ligaments and collagen fibrils, as well as crack deflection and microcracking. Their observation is linked to the microstructure of the bone when crack growth is in the transverse direction. This again confirms the directional properties in bone.

Yan *et al*[50] have come up with a suggestion that a J integral method be used for the calculation of the toughness of bone. The J integral is a parameter that estimates the energies consumed in both plastic and elastic deformations. Yan has applied the elastic-plastic fracture mechanics to describe the mechanical properties of bone. The result of this study has reported a large increase in the fracture toughness of bone compared to those of earlier studies. Yan's theory proposes that crack deflection and bridging processes absorb energy during fracture and therefore further energy is needed for catastrophic failure to propagate from the plastic deformation region. This has been an important factor in increase in the fracture-toughness calculation and results.

The influence of the storage media also affects the fracture toughness of bone. [51]. Lucksanasombool *et. al* have demonstrated this by the use of a single

notch bend test on bovine bone samples. They investigated the effect of storage by dividing the specimens into three groups. The first was stored in saline solution for a period of 1 week, the second, in alcohol for the same period and the third group was transferred after storage in alcohol for one week to a week long storage in saline solution. The effects of alcohol were considered to be equivalent to reduction of the water content in the bone samples which affects the viscoplastic response of the collagen content in the bone tissue. As a result there was an observed increase in the stress intensity factor and a decrease in the stress distribution resulting in an unstable brittle nature of failure. Lucksanasombool has suggested that storage in a saline solution was preferable as it caused negligible permanent deterioration of the collagen content.

2.4 Failure Mechanisms

The structural strength of bone material has been the focal point of many researchers. Various methods are being used in the determination of structural strength. Density has been used as a measure but density does not measure any known mechanical property. [52]. Geometry and mechanical properties together need to be considered during the quantification of bone strength. Beck has highlighted the issues in clinical procedures for determining bone strength as the current technology widely used does not take into account geometry but only mechanical properties. New research is underway using synchrotron radiation and other noninvasive technologies to accommodate all factors governing bone strength.

Finite Element Modeling approach has also been used to determine the tissue modulus and a number of models have emerged in the recent past. Ladd et al. combined three techniques - mechanical testing, three dimensional imaging and finite element modeling- to distinguish between the contributions of architecture and tissue modulus to the mechanical function of the bones. He used X-ray microtomography techniques from synchrotron radiation to obtain three dimensional images of trabecular bone and used this as a structural input for his finite element modeling to calculate tissue modulus which until then was known to have large errors. There is an error in his work that has been attributed to differences in experimental calculation techniques. In this study, the effect of existing damages was not taken into account but however formed a model which reduced variation in the results. Correlation of the microCT to CT number and bone mechanical properties has also been done by Teo *et. al* [53]. As a non-invasive tool, clinical X-Ray computer tomography has been used to calculate bone density in patients. High density bone is expected to have high mechanical properties but a bone with high density and a disjointed architecture will fail at lower loads. There has been large variance in the use of this technique and this has been attributed to microarchitecture of the bone, which is known to vary with age and disease, as it only uses quantitative architectural properties. Teo and his research colleagues in this study have also shown that it is possible that along with density measurements, bone microarchitectural properties can also be predicted using the clinical CT imaging technique.

Follet *et al* [54] have also attempted finite element modeling using synchrotron radiation to determine the intrinsic mechanical properties of bone.

With experimental results from compression tests they compared their results from a finite element model created using the microCT from synchrotron radiation. They found that the numerical Young's modulus is lower using the skeletal model than that of a hexahedral model. This difference has been explained by the building technique used by Follet and his co-workers as apparent mechanical properties are related to partial bone volume.

Bevill *et al* [55] have quantified the influence of large-deformation failure mechanisms and the influence of bone volume fraction and architecture in human bone. Geometrically nonlinear finite element analysis is essential to describe failure mechanisms such as large-deformation bending and buckling. Bevill's study has shown that the use of large-deformation failure criteria has considerably reduced the strength of bone but there is a high dependency on the volume fraction of the bone. Also the magnitude of the strength reduction was correlated to the architectural metrics such as the structure model index, thickness and connectivity density in bones. Although the model describes bone strength in a new perspective, extending the model in experimental work is impossible.

However at the macro scale, a number of experiments have been attempted to better understand the failure behavior of bones at this level of hierarchy. Various testing methods have been reviewed by Beaupied *et al* [56] to provide the advantages and disadvantages of methods extensively used for the evaluation of intrinsic and extrinsic mechanical properties of bones. The extrinsic parameters are obtained from direct test results during testing for the ability to withstand torsional, compressive, tensile and bending forces. These parameters

are known to vary with the geometry of the samples. Intrinsic parameters are computed from extrinsic data and the geometry of samples thereby making the intrinsic parameters independent of the geometry of the samples. Beaupied has insisted on the choice of the test for the computation of the mechanical properties to be selected according to the source of the bone, its nature and the geometry and the loads that are encountered in real life.

Kasra and Grynypas [57] have elucidated the effect of bone marrow and the strain rates on the shearing behavior of bones when subjected to torsional loading. The presence of bone marrow during testing has been proved to be an important factor influencing the stiffening of bones. Bone marrow was found to have a lesser stiffening effect in torsion compared to that in compression. Kasra has also described that the trabecular bone strength is less likely to be dependant on apparent density and more dependant on the strain rates in torsion when compared to that in compression. In addition, the compressive properties are more likely to be vulnerable to bone loss than the shear properties.

The influence of loading rate and damage accumulation in bones on cyclic deformation behaviour has been described by Fleck and Eifler [58], who have observed that the deformation behavior of cortical bone was characterized by the stiffening mechanism and non-elastic linear strain. Load increase tests have been used to discriminate the influence of loading velocity, loading level and thereby of the deformation mechanisms on the mechanical properties. They showed through their study that cyclic creep behavior and partial time dependency is present during recovery in bone material and during low loading steps. Non

linear elastic strain has been attributed to time dependant elastic and plastic deformation as well as crack formation and growth.

The non linear processes of bone material behavior have prompted the use of cohesive zone models in the modeling of fracture on bone material. These models represent the non linear deformation processes involved in fracture by cohesive tractions exerted by the failing material along a fracture process zone rather than attributing all damage to a process occurring at a single point as in conventional linear-elastic fracture mechanics (LEFM).[35]. The cohesive law therefore is a representation of the complete mechanics of bone failure rather than single parameter fracture toughness and therefore provides a superior measure of bone quality. The use of LEFM to model fracture behaviour and processes in bone material is known to generate an error of up to 40% in calculating two data sets from specimen with size variations. For LEFM to be accurate, the crack length and specimen length are to be greater than the process zone length, which is an order of magnitude influenced by the characteristic length. These conditions are impossible to meet in any transverse fracture in bones during the experiments as the sample length is governed by the nature of the bone and the species it is derived from. Therefore the parameters calculated from the LEFM experiments which form material constants are to be dependant on the geometry of the specimen and the crack configuration. A procedure has been suggested by Yang et al. in which the load- displacement fracture data are directly used in the calculation of the mechanical parameters of the bone needed to analyze the fracture data.

Although there has been qualitative and quantitative work done at various levels, there is limited knowledge of bone fracture on the surface and a lack of literature relating to surface strain evolution. The use of optical metrology methods is essential in the study of surface strain in bones. Barak *et al.*[59] have reviewed the various studies involving optical metrology methods in bone studies. Optical metrology methods form an alternative approach to measure displacements on the surface of bones and the advantage lies in doing so without any contact with the test specimen. The various deformation measurement techniques used thus far are holographic interferometry, electron speckle pattern interferometry and digital image correlation methods. These optical interferometry techniques are widely used in the study of metals and composite materials but have not found much interest in bone studies as yet.

2.5 Current Study

The motivation for this research project is derived from the lack of experimental and computed data on strain evolution in bone studies and also the lack of data on the effect of the physiological conditions of the bones during testing. Studies thus far having been limited largely to classical test methods, these methods deliver only integral information of the tested specimen but do not provide localized processes which could provide insight into failure behavior previously misunderstood or misinterpreted. The optical metrology methods provide an alternative to these classical techniques and also provide for a means of testing whole bones. The visualization of the surface strain evolution in whole

bones is essential in understanding the mechanical properties at the bone-muscle interface.

Through this project the research aims to have significant results by:

- Providing bone researchers with an enhanced understanding of sample preparation methods and the effects of sample preparation techniques on the mechanical properties of bones
- Providing bone researchers who use microindentation with an enhanced understanding of the material properties and an understanding of the indentation residual impression
- Providing bone researchers with new information on the effect of the physiological conditions of bones during microindentation
- Providing a novel technique for the characterization of strain evolution during compression and three-point bending of bones. We intend to demonstrate, through the course of this thesis, an approach to study crack propagation and surface strain characteristics of bone.
- Providing the effects of sample size and strain rates on the surface strain measurements and failure behavior of bone materials.

CHAPTER 3

SAMPLE PREPARATION: EFFECT ON MECHANICAL PROPERTIES

3.1 INTRODUCTION

Cleaning of bones for the purpose of osteological examination is a common practice in zoology, anthropology, forensic medicine and pathology [62]. The ability to remove soft tissue from skeletons without compromising bone surface morphology or bone integrity is often paramount. Common methods for cleaning of bones are manual cleaning, enzymatic maceration, cooking, water maceration and insect consumption [62]. Enzymatic maceration that employs digestive enzymes such as trypsin, pepsin, or papain [63, 15] is considered the most convenient method. To enhance the cleaning capability, inexpensive and easily available laundry detergents can be used at room temperature or elevated temperatures [62]. Studies have shown that cleaning using powdered detergents allowed the largest segments of DNA to be clearly identified. It may have less degradative effects on bone DNA than either boiling bone or bleaching processes [64, 65]. In fact, sample preparation techniques affect the microstructure and mechanical properties of human tooth hard tissue [23], a substance similar to bone but more highly mineralized [66]. However, the influence of the cleaning methodologies on microstructures and mechanical properties using detergent and enzymatic macerations has not been investigated in previous studies and is one of the major thrusts of this work.

Hardness is the ability of a material to resist a permanent indentation and is widely used to determine mechanical properties of materials. Microindentation testing provides an alternative to conventional flexural and tensile methods [17]. It is especially useful when the specimen size is very small. In particular, microindentation can produce microscopic cracks of sizes comparable with the microstructural features of the material [17- 19]. Mechanical properties of bone are related to ageing and remodeling of bone. Bone microhardness has been correlated with important parameters such as mineralization and stiffness. It provides a means of examining the mechanical behavior of bone at the micron scale and averaging the effect of osteonal lamellae, while sensitive to variation in mineral content within bone. With careful selection of the microindentation site, it is possible to obtain material characteristics separate from any effects of porosity [18, 19].

The aim of this investigation was to study the influences of water, trypsin, and detergent macerations on bone microstructures and mechanical properties. Trypsin is an easily available enzyme extracted from the porcine pancreas. It is a serine protease, which breaks down proteins. Two typical laundry powders, one without enzyme, the other with two enzymes, were also selected for the current study. Fresh lamb femurs were used as bone samples due to their common use as samples for bone studies. Lamb femurs also exhibit similar mechanical properties to human bones [67]. The microstructure of the cleaned bones was examined using scanning electron microscopy and their porosities were quantified using image processing software. Microhardness was measured using a Vickers

indentation tester to provide an indication of the mechanical properties of the bone material.

3.2 EXPERIMENTAL PROCEDURES

3.2.1. Removal of Soft Tissues

Three maceration fluids containing different additives and water of 2 liters were evaluated as seen in Table 3.1 and compared with the same amount of additive-free water. Solution A was additive-free water. Solution B contained 20 g of trypsin (Sigma Aldrich, Australia). The molecular weight of trypsin is 23800 consisting of 223 amino acids. The pH value of trypsin solution was 7.8. Solution C contained 40g enzyme-free Surf laundry powder (Unilever, Australia). The pH value of Solution C was 11. Solution D contained 40 g Biozet laundry powder (KAO, Australia). Biozet laundry powder contains two types of enzymes for biologically active cleaning: anionic and nonionic surfactants for lifting dirt from clothes, sodium perborate monohydrate for oxygen bleach, sodium aluminosilicate for softening water, sodium carbonate for breaking up fatty soil, fluorescers for brightening fabric, and a soil suspending agent (KAO, Australia). The pH value of Solution D was 10.5.

Solution	Additive	pH Value
A	2 l water only	7
B	20 g trypsin powder in 2 l water	7.8
C	40 g Surf powder in 2 l water	11
D	40 g Biozet powder in 2 l water	10.5

Table 3.1. Test Solutions

Sixteen fresh lamb femurs from six-month old lambs purchased from a local market were stored in a refrigerator at -20 C° before all the joints were cut off using a diamond saw machine. Four femurs were macerated in each solution stored in a closed plastic container for five days at room temperature in a fume cupboard. After five days, manual mechanical removal of soft tissues was conducted using a rod, a cooking knife, and a brush. Care was taken to avoid scraping, scratching or cutting of the bone surfaces. For purpose of safety, all the manual removal was conducted in the fume cupboard. To evaluate maceration of bones for soft tissue cleaning, there are several aspects to be considered including odor, soft-tissue texture, ease of flesh removal and bone quality [62].

The cleaned bone samples were stored in an isotonic phosphate buffered saline (PBS) solution with sodium azide as preservative at room temperature. This solution, containing the identical mineral content to mammalian cells, was prepared by dissolving 800 g NaCl, 20 g KCl, 144 g Na_2HPO_4 , 24 g KH_2PO_4 and 0.2% NaN_3 in 8 l of distilled water, and topping up to 10 l. The pH of the solution was approximately 6.8.

3.2.2. Preparation of Thin Sections

Each femur macerated in each solution was processed for microstructural analysis by scanning electron microscopy following a standard protocol for thin section preparation. A suitable size slab was cut with a diamond saw from the center part of each femur for mounting on a slide. The slab was labeled on one side and the other side was lapped flat and smooth first on a cast iron lap with 400 grit carborundum, then finished on a glass plate with 600 grit carborundum.

After drying on a hot plate, a glass slide was glued to the lapped face of the slab with epoxy. Using a thin section saw, the slab was cut off close to the slide. The thickness was further reduced on a thin section grinder. A finished thickness of 30 μm was achieved by lapping the section plate with 600 grit carborundum by hand on a glass, and followed by fine grinding with 1000 grit. Finally, the section was placed in a holder and spun on a polishing machine using nylon cloth and diamond paste until a suitable surface finish was achieved for microscopic study.

3.2.3. Microstructural Analysis and Porosity Measurement

The thin sections were carbon-coated and were observed under a scanning electron microscope (Cambridge 360, Cambridge, UK). Back-scattered images were taken under high vacuum at 20 kV. The regions of interest on the SEM images were transferred into commercial image processing software (Analysis, Soft Imaging System) in order to perform pore analysis. Each pore area was labeled numerically. The mean pore area sizes were calculated on a representative region with an area of 106875 μm^2 . The porosity expressed in percent was defined by the ratio between the total areas of the pores divided by the total area of the representative region [21]. On each thin section obtained from each femur macerated from each solution, three random locations were measured to obtain the mean value and the standard deviation. Analysis of variance (ANOVA) at a 5% significant level was applied for statistical analysis of porosities.

3.2.4. Standard Microhardness Indentation Testing

Transverse sections with 10 mm thickness were obtained from the central femurs macerated in the four fluids using a diamond saw machine at a low rotary speed. During the cutting process, alcohol was applied as coolant. The 10 mm sections were cleaned to remove any abrasives from diamond cutting and then were preserved in PBS solution. Transverse cut specimens were polished using metallographic polishing techniques. Initial polishing was performed on a series of silicon carbide papers with grit sizes of 240, 320, 400, 600, 800, and 1200. Fine polishing was performed using diamond suspension slurries with grades of 6, 3, 1, 0.25 μm on polishing cloth. The specimens were cleaned using water after different stages of polishing before proceeding to the next finer level of polishing. After final polishing, bone samples were stored in the PBS solution at room temperature.

The polished bone surfaces were indented with a Vickers diamond indenter in a standard microhardness tester (MHT-1, Matsuzawa Seiki, Japan). Five indentation loads of 0.245, 0.49, 1.96, 4.9, and 9.8 N were applied during a loading time of 10 seconds. Six indentations were made at each load on each sample. This resulted in a total of 30 indentations in each sample. A distance of at least two times the impression diagonal was maintained between the indentations to minimize interactions between neighboring indentations. The indentations were completed within 45 min from the time each bone sample was taken out of the PBS solution. The indentation diagonals were measured with optical microscopy. Three samples from the same maceration were selected for

repeat tests. Analysis of variance (ANOVA) at a 5% significant level was applied for statistical analysis of hardness values.

3.3. RESULTS

3.3.1. Removal of Bone Soft Tissues

All the bone samples showed appreciable changes after 5-day maceration in each solution at room temperature. All the marrows were easily removed using a wooden rod and a brush. The soft tissues of the bone samples macerated in Solution A (water) were difficult to remove. Cleaning was conducted carefully by scratching the soft tissues using a knife. The soft tissues of the bone samples in Solution B (trypsin) became completely separated and could easily be removed with a scouring pad without any damage to the bone surfaces. The bone samples macerated in Surf (Solution C) still showed a large amount of soft tissue adhered to bone surfaces, while the samples treated with Biozet (Solution D) were almost soft tissue-free and the remaining tissue could be removed easily.

A noxious chemical odor was associated with the samples macerated in water and trypsin. In particular, the bone samples treated in trypsin were found to be extremely malodorous. The smell of bone samples treated with Biozet and Surf laundry powders was much more acceptable. In particular, the bone samples macerated in Biozet had a pleasant scent.

3.3.2. Microstructure

The SEM micrographs demonstrating the microstructures of the bone samples prepared in each solution are shown in the figure below.

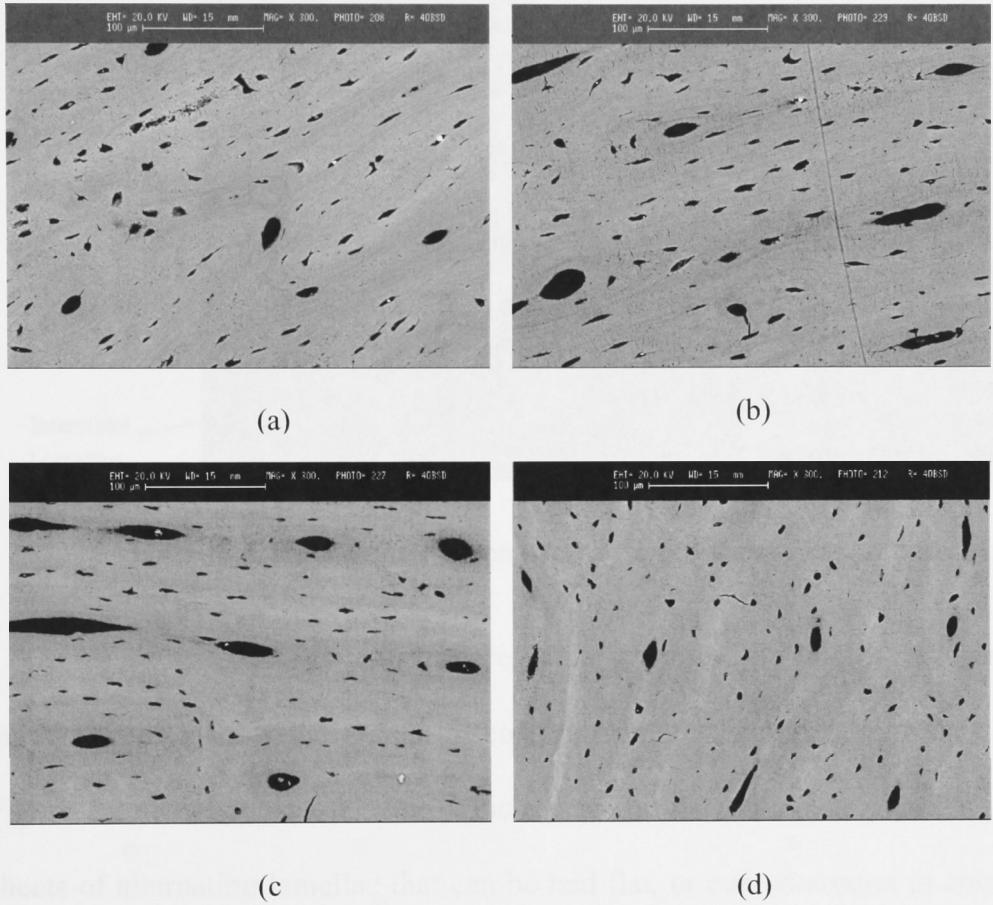


Figure 3.1: Scanning electron micrographs of microstructures of the bones macerated in (a) Solution A (water only), (b) Solution B (with trypsin), (c) Solution C (with Surf) and (d) Solution D (with Biozet).

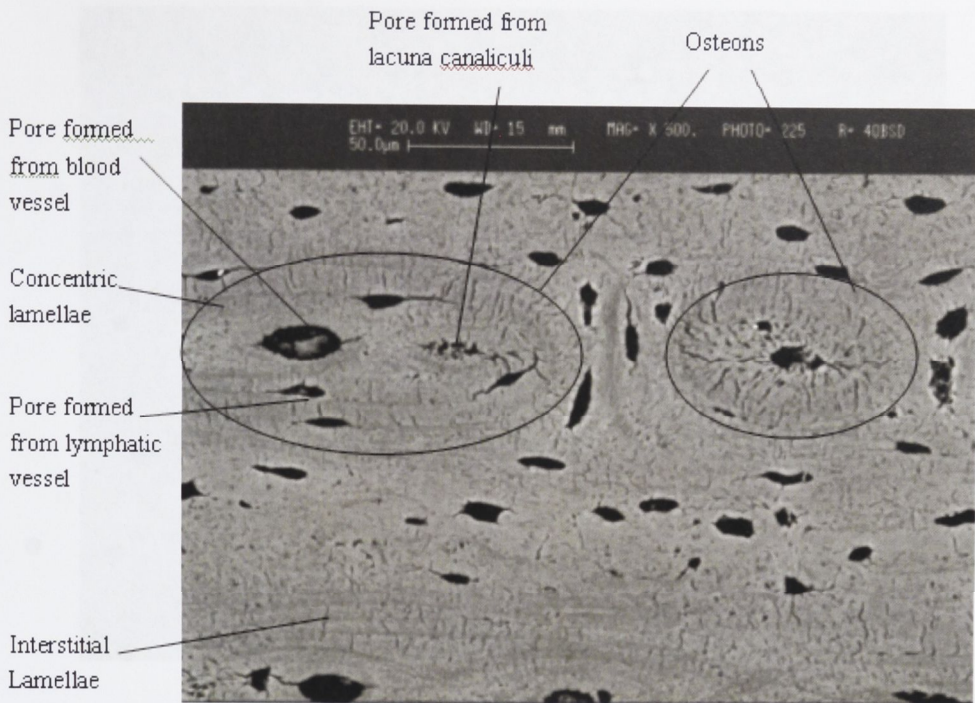


Figure 3.2: High-magnification microstructure of the compact bone,50x

There are no visible differences among these four microstructures. All microstructures show the typical osteonal structure of compact (cortical) bone. Figure 3.2 shows typical osteons, which were formed rather like plywood, from sheets of alternating lamellae that can be laid flat, or curved around in circles to protect blood vessels. The osteons took the form of planar ellipses. One had a major axis of length approximately 100 μm and a minor axis of length of approximately 50 μm . The pores with diameters larger than 10 μm were formed from haversian canals or blood vessels. Smaller pores were formed from lymphatic vessels and lacuna canaliculi. Figure 3.3 shows details of woven bone structure and interstitial lamellae structure.

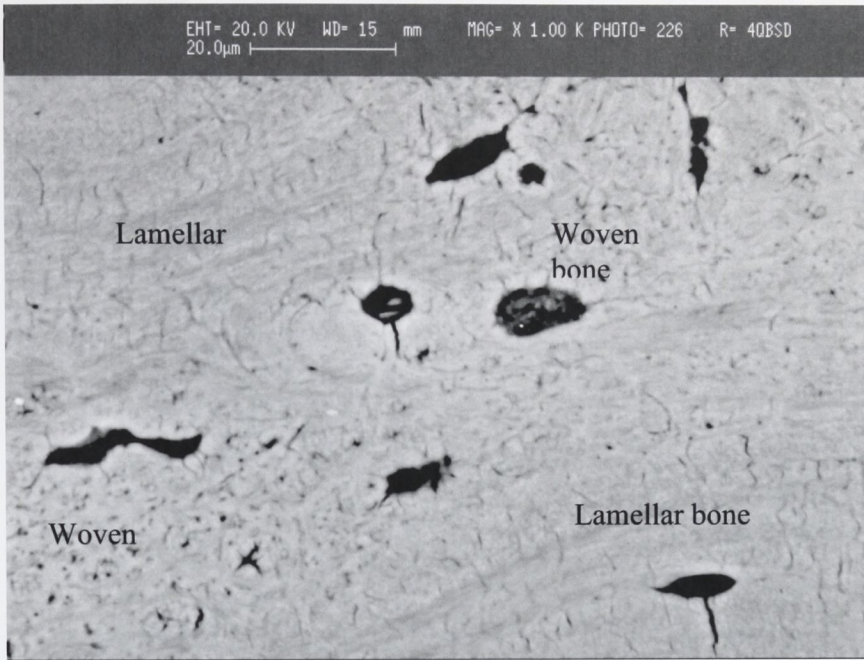


Figure 3.3: High-magnification of woven and lamellar structures,1000x

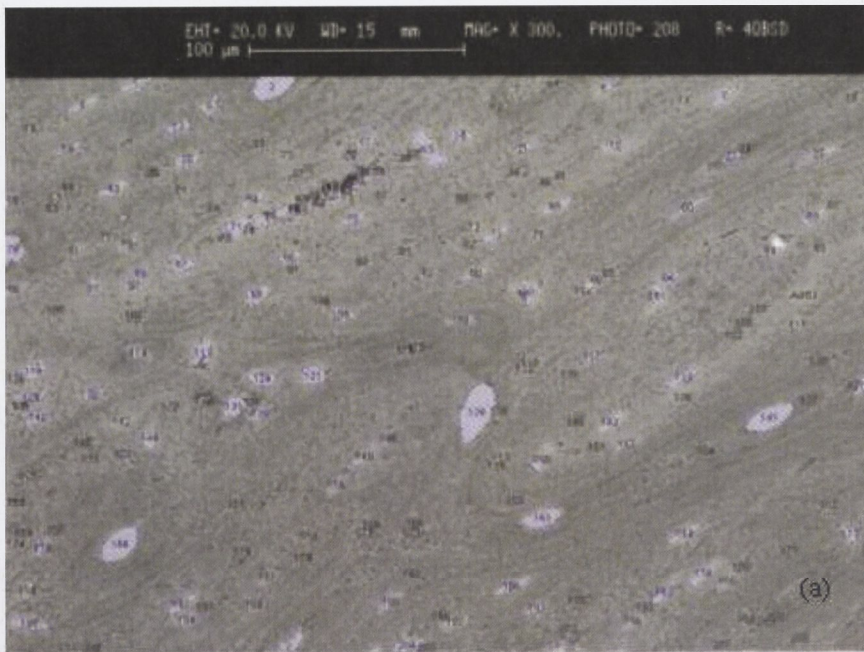


Figure 3.4(a): Porosity identification,300x

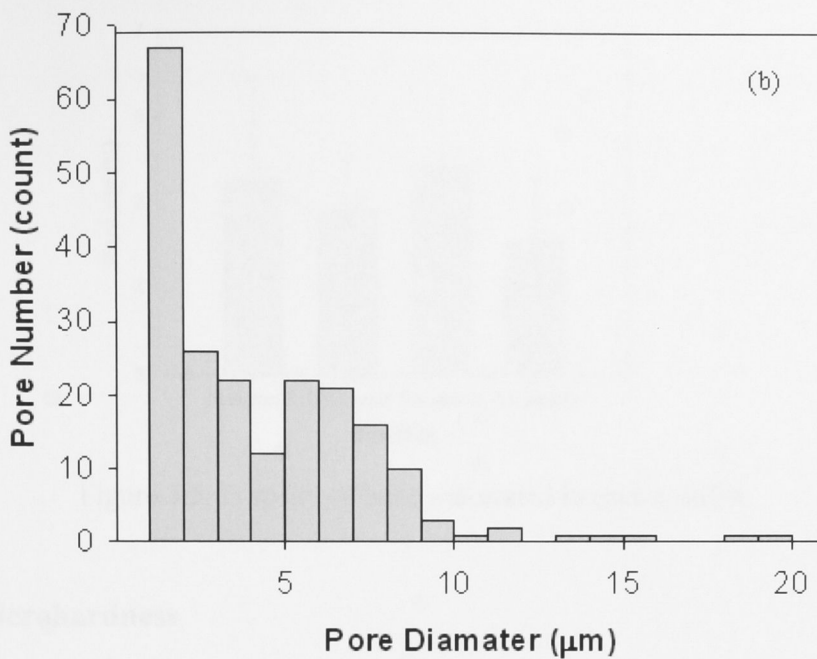


Figure 3.4(b): Typical distribution of pore diameters

Figure 3.4(a) demonstrates one example of identification, analysis and calculation of the porosity in a region of interest. Figure 3.4(b) shows pore size distribution in the region, indicating that 4% pores had diameters of 10–20 μm and 96% of the pores had diameters smaller than 10 μm . The porosities measured for the bones prepared under different macerations are plotted in Figure 3.5. Each datum is the average with one standard deviation of 3 measurements at random locations of the bone sample. The mean porosities of bones macerated in water, trypsin, Surf, and Biozet were 5.3%, 4.9%, 5.3% and 4.6%. Statistical analysis indicates that there is no significant difference among the porosities of bones macerated in different solutions (ANOVA, $p > 0.05$).

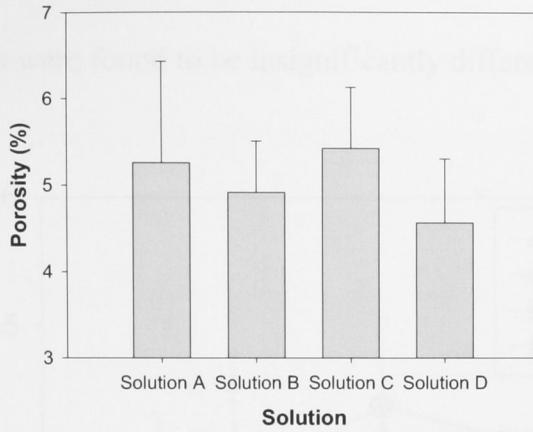


Figure 3.5: Porosity of bone macerated in each solution

3.3.3 Microhardness

Indentation Force (N)	Vickers Hardness (GPa)			
	Solution A	Solution B	Solution C	Solution D
9.8	0.42 ± 0.02	0.39 ± 0.02	0.37 ± 0.07	0.39 ± 0.04
4.9	0.41 ± 0.03	0.41 ± 0.03	0.34 ± 0.08	0.44 ± 0.07
1.96	0.40 ± 0.04	0.37 ± 0.03	0.38 ± 0.09	0.38 ± 0.07
0.49	0.39 ± 0.04	0.30 ± 0.05	0.34 ± 0.06	0.34 ± 0.06
0.245	0.36 ± 0.03	0.30 ± 0.05	0.30 ± 0.05	0.35 ± 0.06

Table 2. Standard microhardness indentation results

The results from microindentation tests are listed in the table above. Each datum is the average with one standard deviation of 18 indentations in 3 samples.

Figure 3.6 demonstrates the Vickers hardness against the applied load for the bones macerated in different solutions. At the lower loads of 0.245 N and 0.49 N, all the hardness values of the bones macerated in the different solutions were not significantly different (ANOVA, $p > 0.05$). At the higher loads of 1.96–9.8 N, values were not significantly different (ANOVA, $p > 0.05$). However, at the lowest load of 0.245 N, the hardness values of the bones macerated in the different solutions were significantly smaller than those at the highest load of 9.8

N (ANOVA, $p < 0.05$). For the bones macerated in the different solutions, their hardness values were found to be insignificantly different (ANOVA, $p > 0.05$).

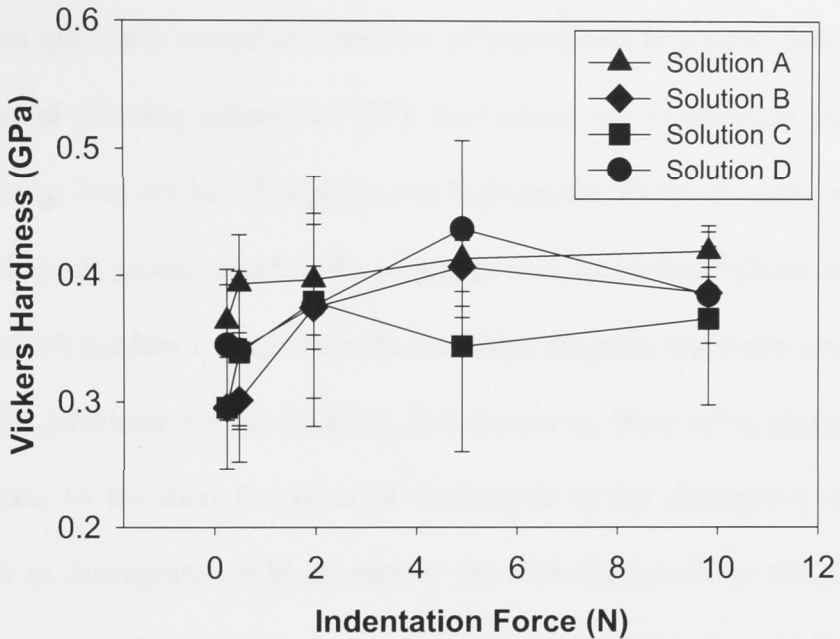


Figure 3.6: Vickers hardness of bones macerated in the different solutions

3.4. DISCUSSION

Soft tissues of bone mainly contain organic protein, fat and collagen [68]. Bone marrow is the tissue comprising the center of the medullary cavity and contains a rich vascular network and a series of cells that may produce blood cells (red bone marrow) or be transformed into fat (yellow bone marrow). All these soft tissues are essentially macromolecular substrates [22].

Water maceration at room temperature is traditionally considered the safest method for bone as no heat or chemicals are applied that may disrupt bone integrity, but the process of degradation of protein to reduce the soft tissue was notoriously malodorous. Enzymes, on the other hand, digest a macromolecular

substrate and exemplify an important category of hydrolytic reactions [35]. Trypsin is one of proteolytic enzymes that can attack the peptide molecule, whereas the exopeptidases hydrolyze the terminal peptide bonds [26]. Laundry detergents generally comprise a mixture of ingredients in which surfactants are the essential cleaning substances [27]. Surfactants are compounds that have a dual affinity; they are both lipophilic and hydrophilic. Their molecule consists of a lipophilic tail group, which links to greasy soil, and a hydrophilic polar head group, which renders it water-soluble and helps disperse and rinse away greasy soil [27]. Mechanisms for cleaning soft tissues in bone using detergents are mainly due to the dual functions of surfactants in the detergents. Additional enzymes in detergents could accelerate the cleaning speed by the enzymatic action to break the proteins in bone soft tissues. Thus, the detergent with enzymes at room temperature produced the best cleaning results.

The compact or cortical bone is essentially solid material, in which spaces for blood vessels and living cells give it a porosity of about 5%. It makes up the majority of long bones [16]. The primary mineral material in bone is crystals of hydroxyapatite, a hard, brittle mineral material based on calcium phosphate [28-30]. It is unlikely that enzymes or bacteria could react with such a mineral. Given that all the solutions applied in this study had pH values above 7, it is likely that cleaning with water, trypsin, and detergent macerations could only remove the organic structures in bones, with little if any effect on the mineral structure of bone, which determined the mechanical properties.

Porosity plays a significant role in bone microstructure. Pores in bone are mainly formed from intrasosseous capillaries and Volkmann's canals of larger

diameters, and canaliculi of much smaller diameters. Figure 3.3 and Figure 3.5 shows that the pores formed from intrasosseous capillaries and Volkmann's canals with diameters of 10 μm or larger constituted less than 5% of pores. 95% of pores were formed from canaliculi, the tiny channels which run through the laminae that comprise the osteons.

Cortical bone composition and structure can vary significantly and influence the tissue's mechanical properties [31]. In the current study, the macerations in different solutions did not cause a change in porosity (Figure 3.5). Also the bone microhardness was not influenced by the different macerations (Figure 3.6). Generally, porosity, mineralization, bone matrix, and microstructure seldom vary independently. They are usually observed to change simultaneously [47]. Noticeably, the hardness was significantly lower at the lowest load than that at the highest load (Figure 3.6). For engineering materials such as ceramics or metals, the hardness-load curve is often referred to as the indentation size effect, which follows the Meyer's law [32]. Hardness versus load is either constant or decreasing with load or the hardness has an abrupt transition of a constant value [32]. For bone, however, hardness versus load shows an increase with load (Figure 3.6) with a transition of an abrupt constant value at the load of 1.96 N. Unlike single crystal, polycrystals or amorphous structures in engineering materials, bone is a composite of a fibrous polymer (organic collagen fibers) matrix reinforced by ceramic nanoparticles (inorganic carbonated hydroxyapatite) [69]. The collagen fiber matrix exhibits high toughness and elasticity while the crystallized hydroxyapatite is very brittle. In indentation, bone materials behave not only in a brittle manner but also exhibit viscoelastic

behavior [33]. We have observed a certain degree of recovery at the indentation sites of the applied loads. This rate dependent effect will be a focus of our future study.

3.5. Summary of Sample Preparation tests

- Most commonly used preparation methods were identified and analyzed
- Samples macerated in Trypsin showed faster preparation times
- Samples macerated using Biozet detergent had lesser smell and comparatively faster preparation time than water
- All preparation methods showed no significant changes on microstructure
- No significant changes were observed

Chapter 4

MICROINDENTATION OF BONE: EFFECT OF PHYSIOLOGICAL CONDITION

4.1 INTRODUCTION

Cortical bone has a strong hierarchical structure, in which there are phase and material direction changes over many length scales and a porosity of about 5% due to the presence of blood vessels and living cells [24]. These heterogeneities account for the ability of bones to contain stable cracks that can vary greatly in length. It is very difficult to determine at what level the processes leading to failure occur due to the complicated interactions between heterogeneities and microcracks when considering failure behavior [16]. The effects of microstructure of bone on crack propagation and mechanical properties need to be investigated [16].

Indentation tests represent a promising direction in characterizing the quality of bone repair as a function of location [15, 35, 26- 28]. These tests have been used to measure local mechanical properties of callus and the surrounding tissues [29- 31]. Hardness is the resistance of a material against deformation under indentation by an object. The advantage of hardness tests is that these tests can be done on very small specimens [15]. Microhardness is measured from the penetration of an indenter, which makes imprints of microscopic size, thus allowing the determination of hardness in small areas of the sample. Previous studies using microindentation mainly focused on microhardness anisotropy of compact bone [27- 32] and hardness measurement of human enamel and dentine [33, 34].

Microindentation provides a basis for evaluating a range of contact-related properties, particularly surface-damage phenomena in sharp-particle compression [34].

Furthermore, imaging of micro-indented patterns using scanning electron microscopy can provide insight into the material response to mechanical loads at the micro scale to identify the role of microstructure of bone in damage. The aim of this study was to investigate crack propagation and deformation behavior of dry cortical bone on a microscopic scale by means of microindentation. The microcrack-microstructure interactions were examined by evaluating indentation-induced cracks in osteons, interstitial lamellae, and woven fibrils using SEM. We measured the Vickers hardness during indentation using optical microscopy and recovered hardness using SEM. Micromechanistic damage in microindentation of dry cortical bone was identified.

The studies so far do not elucidate the effect of the sample condition during testing or preparation. Therefore, there is a necessity to understand the influence of the sample condition on the mechanical properties of bone. The aim of the current study was to investigate the effects of the sample conditions on the microhardness of lamb femora. The microindentation topographies of both dehydrated or dry samples and wet samples were examined for this purpose. Vickers hardness was evaluated using an optical microscope and was also verified using confocal-laser scanning microscopy.

4.2. EXPERIMENTAL PROCEDURE

4.2.1. Sample preparation

Samples for this study have been prepared as discussed in Chapter 3 using Biozet detergent. Cortical lamb femurs were macerated in a solution containing Biozet laundry powder (KAO, Australia) and were manually cleaned using a knife, a scalpel, and a brush. Transverse-section samples of 10 mm thickness were cut from the central femurs using a diamond saw machine at a low rotary speed. Alcohol was utilized as coolant during the cutting process. The samples were washed to remove any residual abrasives from the cutting. Then, they were polished using polishing techniques similar to those

described in Chapter 3. The samples were then separated in batches of 12 of which half were dried in an oven at 35°C for 2 days to prepare dehydrated bone samples. The rest were maintained in a wet condition by storage in a phosphate buffered saline.

4.2.2. Standard Microhardness Indentation Testing

The polished dry bone surfaces were indented with a Vickers diamond indenter in a microhardness tester (MHT-1, Matsuzawa Seiki, Japan). Five indentation loads of 0.245, 0.49, 1.96, 4.9 and 9.8 N were applied for 10 seconds. Six indentations were made at each load on each transverse section. This resulted in a total of 30 indentations in each sample. A distance of at least two times the impression diagonal was kept between the indentations to prevent the interactions between neighboring indentations. The lengths of the indentation diagonals were measured with optical microscopy. Three samples were selected for repeat tests and production of total 18 indentations at each load. The indented samples were carbon-coated and stored in an oven at 42°C for 48 hours for the purpose of being easily vacuumized in the SEM sample chamber. Samples were observed under an SEM (Cambridge 360, Cambridge, UK). Backscattered electron (BSE) imaging was performed at 20 kV accelerating voltage at a working distance of 16 mm, and 350 times and higher magnifications. Both the optical microscope and the SEM were calibrated prior to the length measurements and had relative system uncertainties of about 2%.

4.3. RESULTS

4.3.1 Micromechanical performance analysis

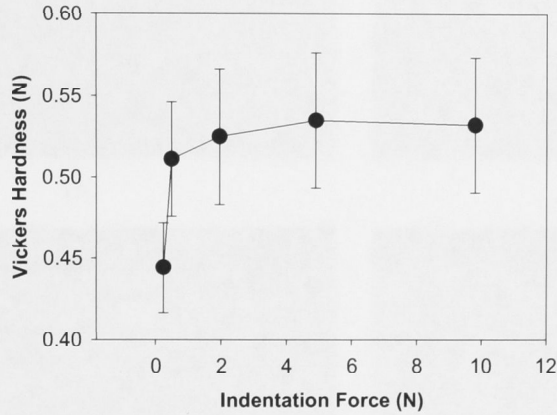


Figure 4.1: Vickers hardness of dry bone

The above figure shows Vickers hardness against applied load. Each datum is the average with one standard deviation of 18 indentations in three samples. It demonstrates that hardness increased with the applied load. In particular, the hardness significantly increased with the load at the low loads of 0.245 N and 0.49 N (ANOVA, $p < 0.05$). After the load reached 1.96 N, hardness was independent of the load (ANOVA, $p > 0.05$). By increasing the load from 0.245 N to 4.9 N, hardness increased by 15% from a mean of 0.45 GPa to 0.54 GPa, whilst hardness values remained approximately unchanged when the load was increased from 1.96 N to 9.8 N.

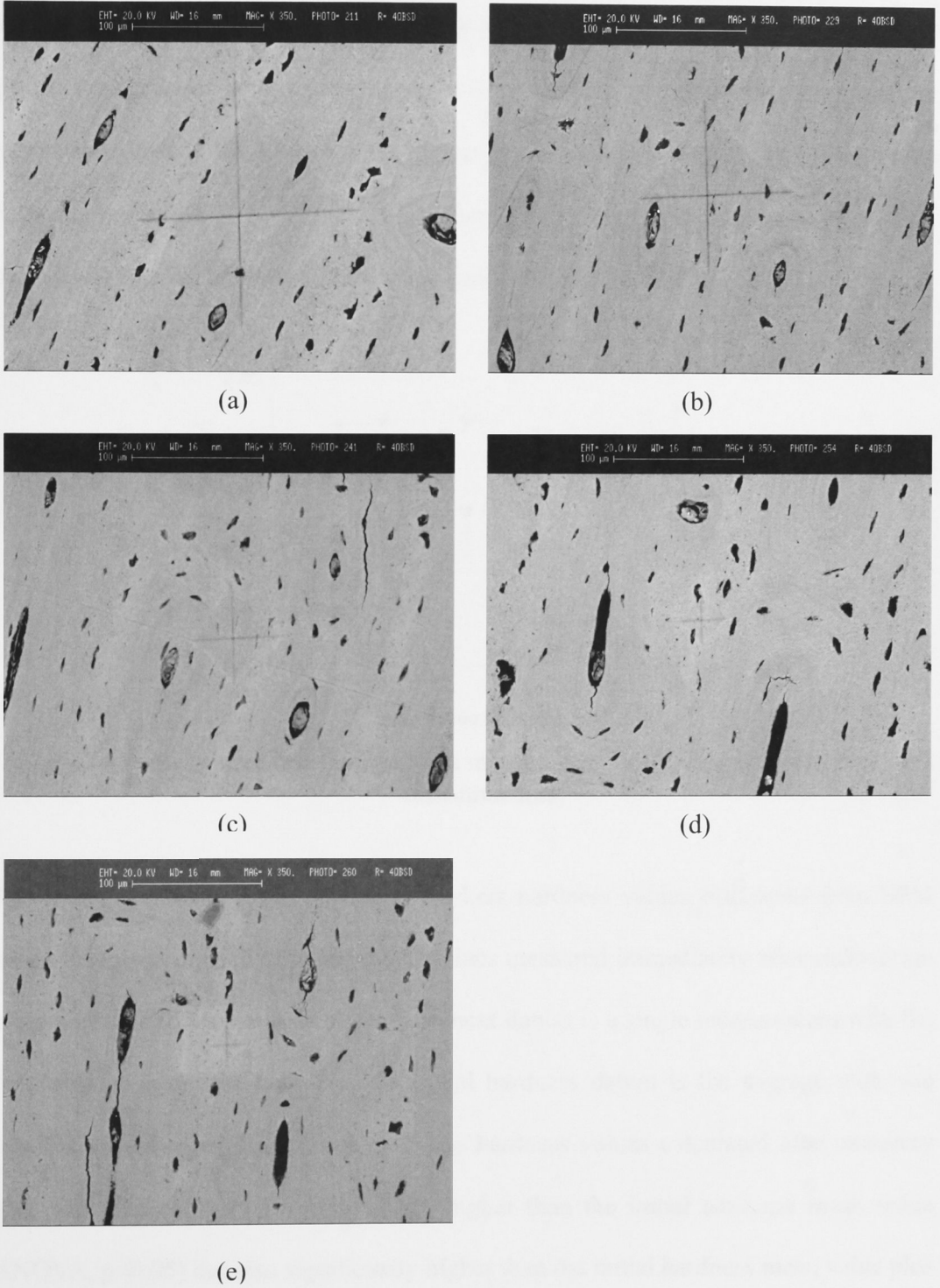


Figure 4.2: BSE images of the indentation patterns at the loads (a) 9.8 N, (b) 4.9N, (c) 1.96 N, (d) 0.48 N and (e) 0.245 N,350x

Figure 4.2 shows a series of backscattered electron (BSE) images of indentation patterns at the applied loads of 9.8, 4.9, 1.96, 0.45 and 0.245 N at 350 times magnification. No cracks are clearly observed on the indentations patterns at any applied load. Plastic deformation is observed in all the indented areas. However, the indentation patterns were found to be apparently smaller by measuring the indentation diagonals under the SEM than the initial hardness indentation measured using optical microscopy immediately after the indentations were made.

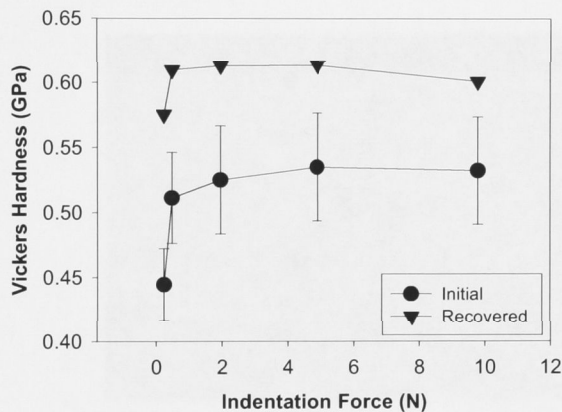
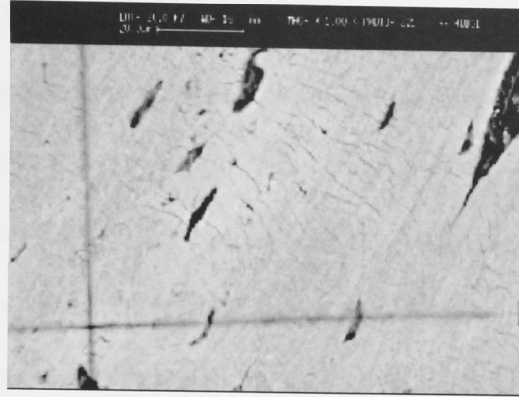
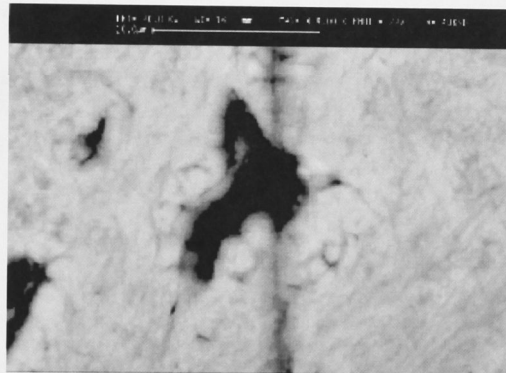


Figure 4.3: Recovered Vickers hardness measured under SEM compared with initial measurements

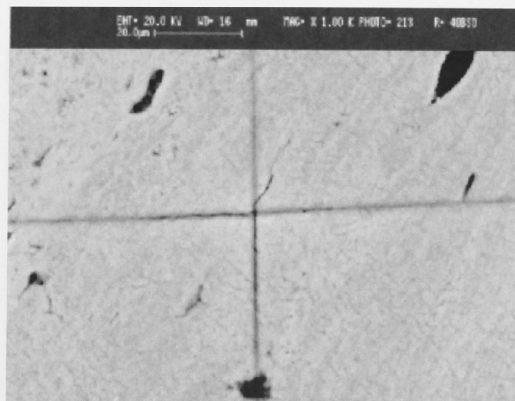
The above graph shows the recovered Vickers hardness values calculated from SEM measurements compared with the initial values measured immediately after indentation in the hardness tester. Each recovered hardness datum is a single measurement with the SEM system error less than 2%; the initial hardness datum is the average with one standard deviation of 18 indentations. The hardness values calculated after recovery were found not only to be significantly higher than the initial hardness mean value (ANOVA, $p < 0.05$) but also significantly higher than the initial hardness mean value plus one standard deviation (ANOVA, $p < 0.05$). In particular, at least 12% recovery of the indentation deformation occurred at loads lower than 0.45 N. At least 5% recovery of the deformed bone was observed at loads higher than 1.96N.



(a)



(b)



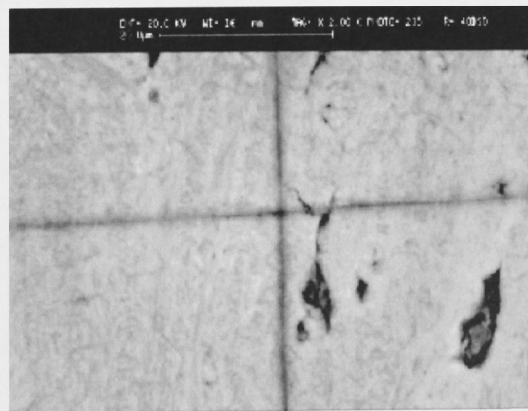
(c)

Figure 4.4: High-magnification BSE images of the indentation patters at the applied load of 9.8 N,1000x

Figures 4.2(a) and 4.2(b) show that at load 9.8 N, the indented area covered several osteons, woven fibrils and interstitial lamellae. To reveal deformation details of the indentations, high-magnification BSE images are shown in Figure 4.4. Figure 4.4(a) demonstrates a microcrack propagated from a large haversian canal with a length of approximately 10 μm . It also shows that microcrack clusters developed from the boundaries of small osteocyte lacunae in the bone, with lengths smaller than 20 μm . Figure 4.4(b) shows microcracks formed in the woven fibrils from a canaliculus, with lengths smaller than 5 μm . Figure 4.4(c) reveals a microcrack developed at the apex of indentation along the longitudinal lamellae.



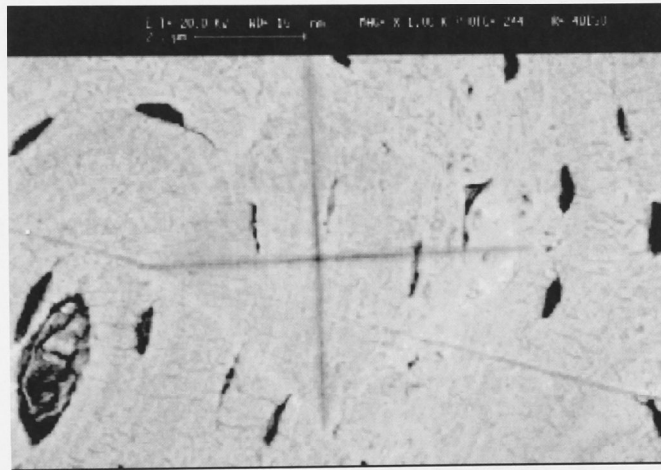
(a)



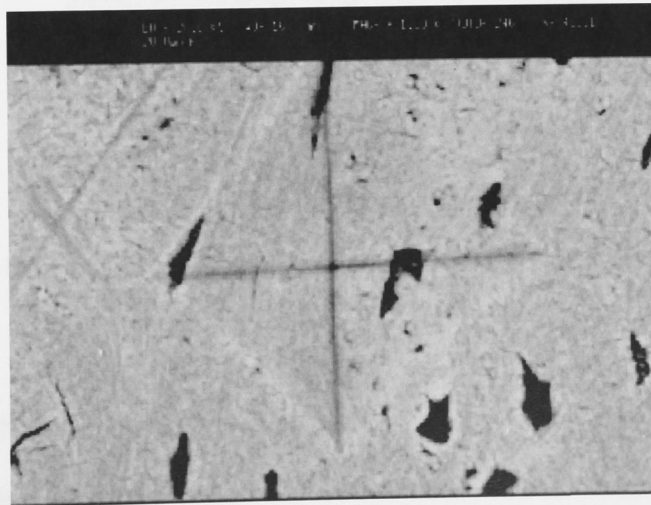
(b)

Figure 4.5: High-magnification BSE images of the indentation patterns at the applied load of 4.9 N, 1000x

Figure 4.5 shows high-magnification BSE images of indentation patterns indented at load 4.9 N. These images show that deformed indentation areas cover both interstitial lamellar, woven, and osteonal structures. Figure 4.5(a) clearly reveals a microcrack with a length of approximately 5 μm , propagated from a large haversian canal. Some microcracks developed from small osteocyte lacunae. Figure 4.5(b) depicts the microcracks propagated from the boundaries of canaliculi with lengths smaller than 10 μm .



(a)



(b)

Figure 4.6 High-magnification BSE images of two indentation patterns at the applied load of 1.96 N, 1000x

Figure 4.6 shows high-magnification BSE images of two indentation patterns indented at load 1.96 N. Microcracks are seen to develop from the boundaries of canaliculi, all with lengths smaller than 5 μm .



Figure 4.7: High-magnification BSE image of the indentation pattern (0.49N), 1500x

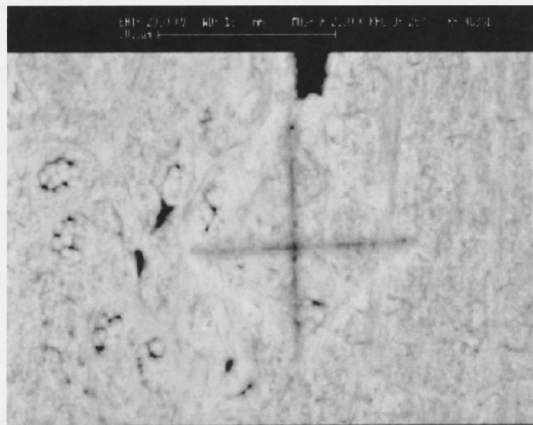


Figure 4.8: High-magnification BSE image of the indentation pattern (0.245N), 1500x

Figure 4.7 shows a high-magnification BSE image of the indentation pattern indented at load 0.49 N. No microcracks could be found to initiate from the boundaries of canaliculi. Figure 4.8 shows high-magnification BSE image of the indentation pattern indented at load of 0.245 N. The indentation deformation is plastic without visible microcracks.

4.3.2 Effect of the physiological condition of samples

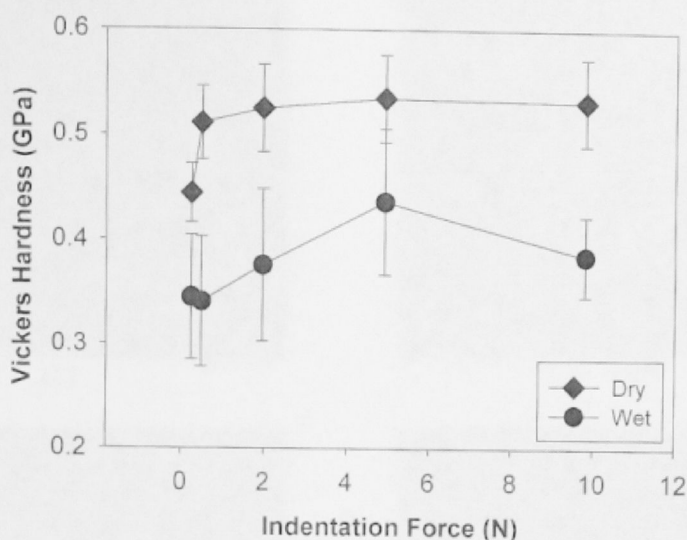


Figure 4.9: Vickers hardness of dry bone and wet bone versus indentation force

Figure 4.9 shows Vickers hardness against applied load. Each datum is the average with one standard deviation of 18 indentations in three samples each of wet and dehydrated cortical bones. Hardness was observed to be higher in that of the dry cortical bone samples than in that of the wet condition. Hardness was found to increase with load at lower loads of 0.245N and 0.49N (ANOVA $p < 0.05$). The hardness remained almost constant in the dry samples while the wet bones showed a decrease in the hardness after the application of the same loads.

Figure 4.10 shows a series of images of indentation patterns obtained from the confocal laser scanning microscopy. The images from 4.10(a) – 4.10(f) are the images of the indentation sites of a dry cortical bone sample from the apex of the indent to the surface of the surface of the sample. Microcracks are visible throughout the indentation site and are observed to be in the direction of the long axis of naturally occurring ellipses.

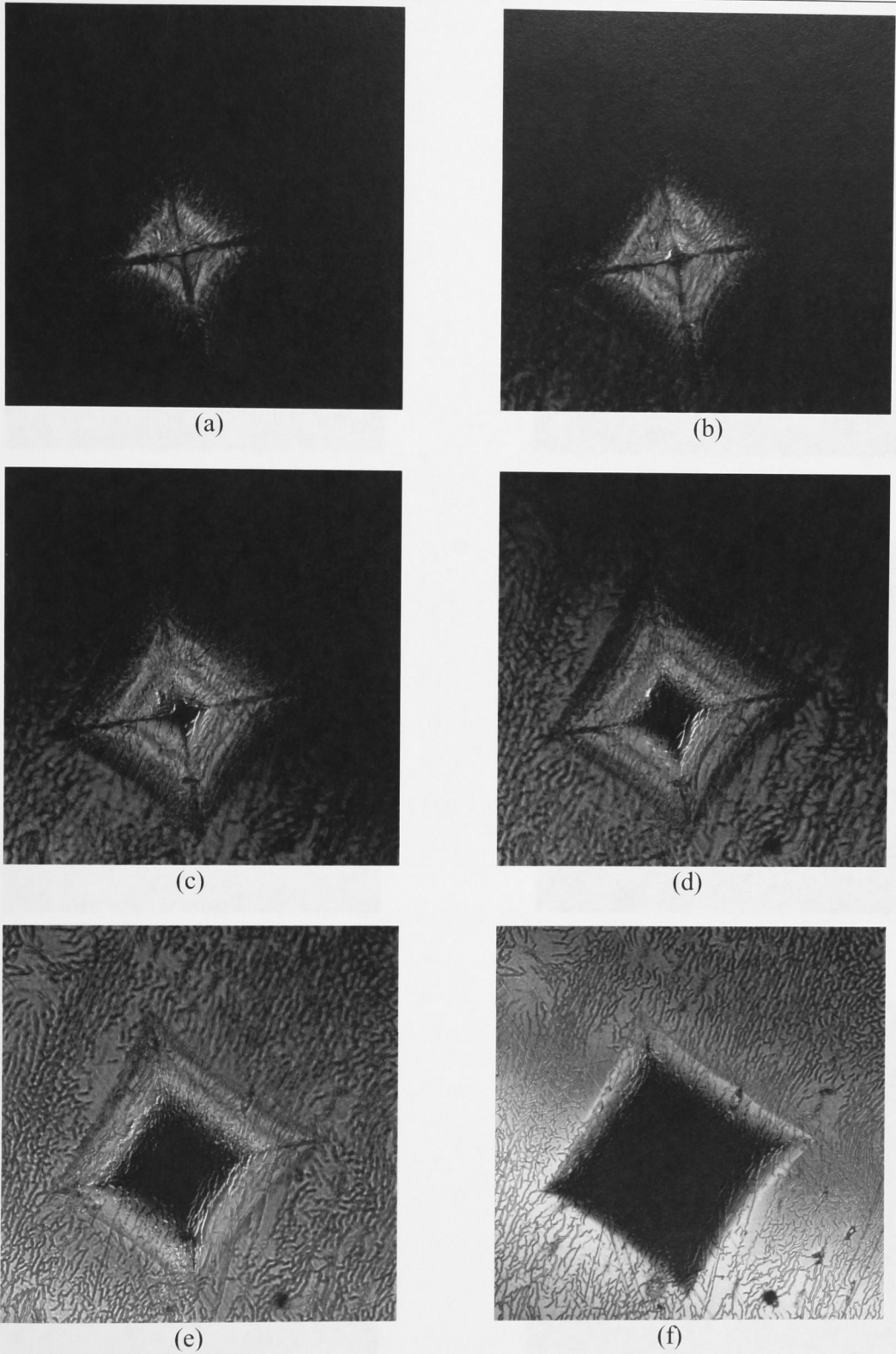


Figure 4.10: Confocal laser scanned images of the indentation patterns at various depths in a dry cortical bone sample,300x

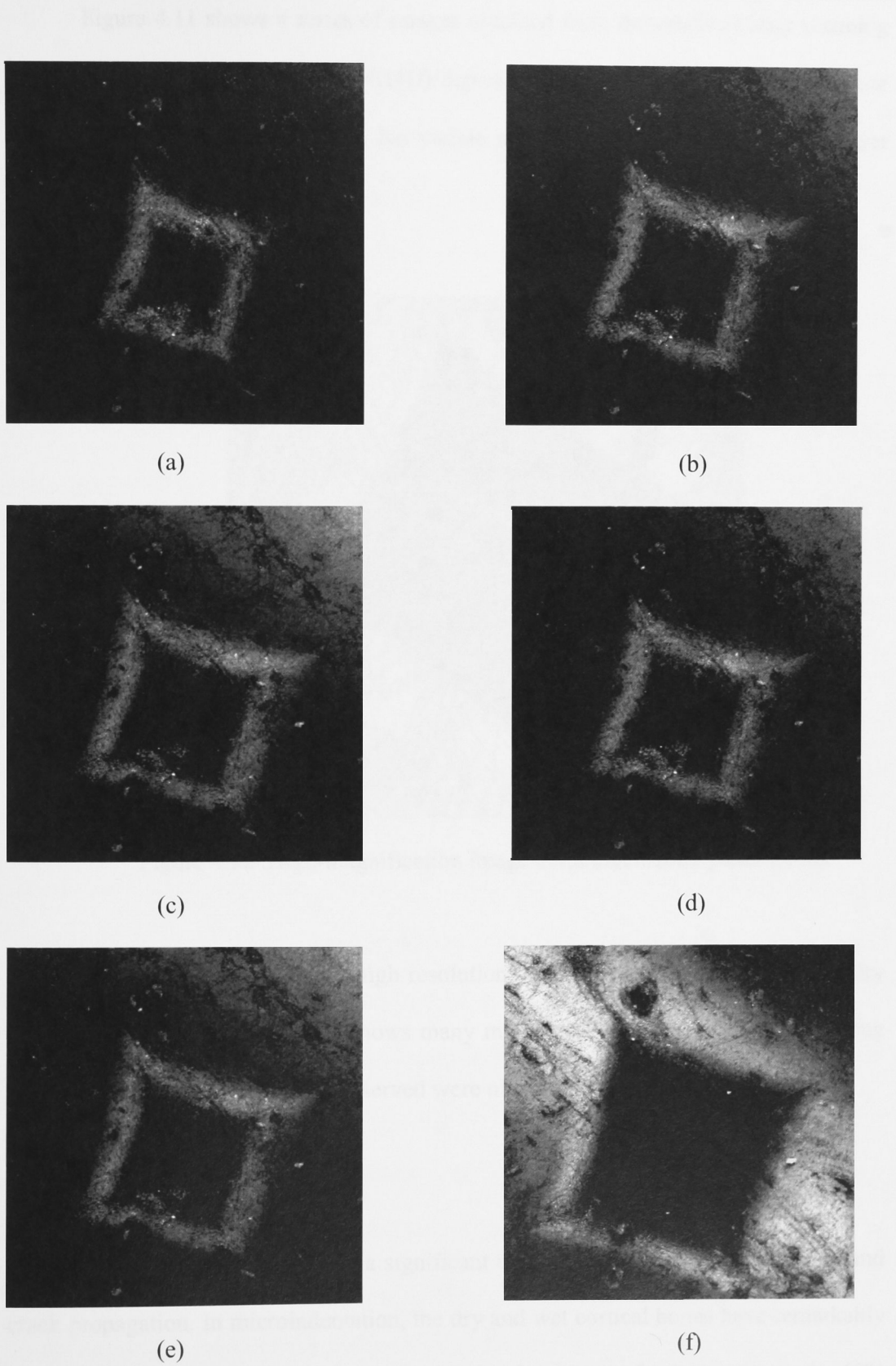


Figure 4.11: Confocal laser scanned images of the indentation patterns at various depths in a wet cortical bone sample,300x

Figure 4.11 shows a series of images obtained from the confocal laser scanning microscopy. The images 4.11(a) – 4.11(f) depict the indentation sites starting from the apex to the surface of the sample. No visible microcracks were observed in the wet cortical bone sample.

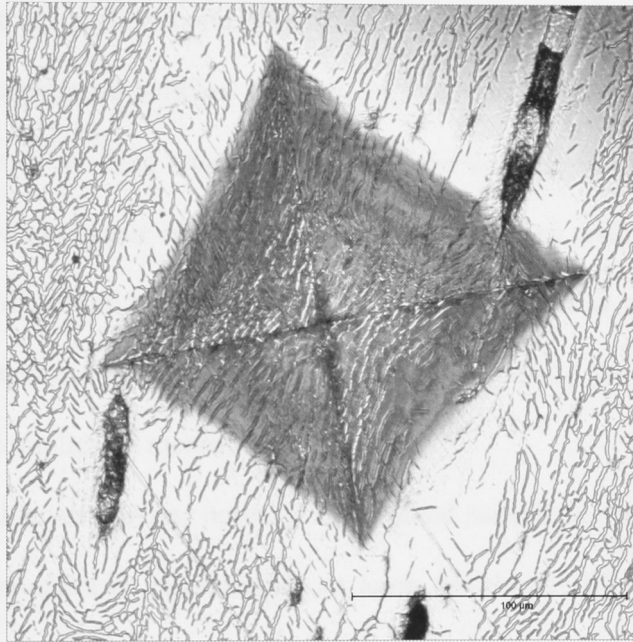


Figure 4.12 :High-magnification image of an indentation pattern,400x

The above figure shows a high resolution image of an indentation site of a dry cortical bone sample. The figure shows many microcracks in the direction of the long axis of the ellipses. Microcracks observed were of a length $10\mu\text{m}$.

4.4. DISCUSSION

The bone microstructure exhibited a significant effect on the mode of deformation and crack propagation. In microindentation, the dry and wet cortical bones have remarkably plastic, viscoelastic and brittle behaviors. Bone is composed of approximately 60% ceramic nanoparticles (inorganic carbonated hydroxyapatite), 10% water and about 30% fibrous polymer matrix (organic collagen fibers) by weight [15]. Polymers are often

able to dissipate energy by viscoplastic flow or formation of non-connected microcracks [17, 21]. Studies have shown that the organic matrix of bone as well as its function in the microstructure could be the key to resist the separation of mineralized collagen fibrils [67]. In ceramics, well-known toughening mechanisms are based on crack ligament bridging and crack deflection [35]. In microindentation, all these phenomena were identified in the dry cortical bone. It is of interest to compare the microstructural responses to microindentation between the cortical bone and dental enamel, both of which are considered as hard tissues. Enamel contains 92–96% of inorganic hydroxyapatite, 1–2% of organic materials and 3–4% of water by weight [70]. Due to the high percentage of ceramic hydroxyapatite, enamel was revealed to be extremely brittle in microindentation with extensive edge chipping and cracks [34] while cortical bone revealed more complicated mechanical behaviors.

In the current investigation, porosity from blood vessels in the cortical bone exhibited a significant effect on microcracks. At loads 4.9 N and higher, the observed anisotropic cracking behavior can be attributed to the weak boundaries of porosities (haversian canals, osteocyte lacunae and canaliculi), in particular, the larger pore boundaries formed from the large haversian canals. The microcracks developed more easily in the direction of the long axis of the planar ellipses of a large-sized pore formed from a haversian canal, as shown in Figure 4(a). The propagation of the microcracks also occurred perpendicular to the long axis of the planar ellipses of the medium-sized pores formed from osteocyte lacunae, as shown in Figure 4(a). Furthermore, microcracks propagated from small-sized pores formed from canaliculi as shown in Figure 4(b). Bone is a hierarchically structured composite. At the indentation apex, microcracks were easily developed along the lamellar layers as shown in Figure 4(c). At loads smaller than 1.96 N, indentation patterns were more plastic than brittle, in which cases the microcracks became smaller or were not observed.

Another direct observation is the significant recovery of indentation deformation as shown in Figure 4.3. In particular, at lower applied loads than 0.45 N, the bone exhibited more viscoelasticity than that at high loads. Bone recovery following microindentation was also observed in wet bovine femur [71]. This time dependence of viscoelasticity in bone was observed in R-curve testing of human cortical bone as well [73]. Time-dependent crack growth occurred in bone under sustained (non-cyclic) *in vitro* loads at stress intensities lower than the nominal crack-initiation toughness [73]. Effects of viscoelasticity and time-dependent plasticity of human cortical bone were further investigated using nanoindentation [72]. However, the exact nature of such behavior is as yet unclear [73].

Hardness was found to increase with load, as shown in Figure 4.9. This phenomenon was also observed in microindentation of dry embalmed human rib [32]. However, in microindentation of wet bovine metacarpus, hardness decreased with the applied load [27]. For engineering materials such as ceramics or metals, hardness versus load is either constant or decreasing with load or shows an abrupt transition to a constant value [74]. Research has found that for natural materials, the widely used engineering concept of stress concentration at flaws is no longer valid due to their many levels of hierarchical structures [18]. Nanoindentation was performed in specific features such as trabecular, interstitial lamellae and thick and thin lamellae in osteons. Hardness and modulus differences among the various microstructural components were also found [75, 76] and were attributed to collagen fibril orientation and anisotropy as well as variation in mineral content [17].

The tissue condition has exhibited a significant effect on the deformation behavior and crack propagation in the cortical bone samples. Bone is composed of approximately 60% ceramic nanoparticles (inorganic carbonated hydroxyapatite), 10% water and about 30% of fibrous polymer matrix by weight. [15]. Polymers are often

able to dissipate energy by viscoplastic flow or non-connected microcracks [17, 19]. It is of our interest to compare the topographies of the microindentation sites of the dehydrated samples and wet samples of lamb femur.

In the current investigation, the tissue condition has exhibited significant impact on the mechanical properties of bone. The dehydrated samples show a large number of microcracks. At loads of 0.49N and above microcracks were observed to develop in the direction of the long axis of the planar ellipses formed by the haversian canals. This cracking behavior describes the anisotropic effect known to exist in bones. Figure 4 shows the propagation of non-connected microcracks in the direction of the long axis of these ellipses. The microcracks also propagated from the edges of the indentation site showing the brittle nature of the dehydrated lamb femur. Another observation was that the indentation patterns were more plastic than brittle at lower loads.

The observations of the wet bone samples indicate plastic and viscoelastic behavior of the bone during the indentation. There were no visible microcracks even at higher loads. This indicates the non brittle behavior of the bones in the wet conditions. Hardness was found to increase with load up to a load of 0.49N and thereon the hardness was observed to reduce. This phenomenon has been observed and has been attributed to the hierarchical structure of the bone. [18].

4.5. Highlights of Microindentation Testing

- Vicker's indentation showed rate dependant and load dependant behavior
- Higher loads showed more brittle mechanical failure
- Lower loads showed more ductile deformation
- A significant recovery was observed in the indentation impressions in 24 hours
- Physiological condition showed significant effect with dehydrated bone samples having higher hardness than the wet samples

- Wet bone samples were found to be ductile in nature while dehydrated bone samples were found to have brittle mechanical properties

COMPRESSION TESTING OF BONE MATERIAL

5.1 Introduction

Bone has been of interest to many professional disciplines such as physics, mechanical engineers and biomedical engineers. The mechanical and material properties are of great importance in these disciplines as they control the behavior of the body in the understanding of their mechanical behavior with the biological structure of bone and recognizing their functions. Although much work has been done over the decades in understanding these properties, certain aspects of these materials are still not fully understood. The bone surface is a key part and plays an important role in maintaining the condition of the whole bone. It also forms the very important interface between the bone and the outside system in the body. It is essential to understand the functioning of this part of bone as it can give us significant information on the characteristics of bones and their functioning in the body. The mechanical testing performed on bone materials of different shapes have provided valuable data and have helped in understanding the system in the body. However, there is a characteristic bone material with a view of understanding the evolution of stress during mechanical loading. The study aims at characterizing the stress behavior using an optical measurement system based on photoelasticity in a real time environment. This Chapter describes compressive test results with the stress distribution on the surface of the bone during the testing. This Chapter outlines

COMPRESSION TESTING OF BONE MATERIAL

5.1 Introduction

Bone has been of interest to many professionals such as orthopedics, doctors, mechanical engineers and biomedical engineers. The properties of bone materials are of most importance to these professionals as they contain information that is the key to the understanding of these materials, dealing with the problems relating to bones and replicating these materials. Although much work has been done over the decades to understand these materials, certain aspects of these materials are not yet fully understood. The bone surface is a key part and plays an important role in maintaining the condition of the whole bone. It also forms the very important interface between the bone and the muscle system in the body. It is important to understand the functioning of this part of bone as it can provide significant information on the characteristics of bones and their functioning in the body. The mechanical testing performed on bone materials of various species have provided valuable data and have helped in understanding the system so far, but little has been done to characterize bone materials with a view of understanding the evolution of strain during mechanical loading. This study aims to characterize the strain evolution using an optical measurement system based on photogrammetry in a real time environment. This Chapter describes compression test results with the strain distributions on the surface of the bones during the testing. This Chapter outlines

experimental methods, sample measurements and a detailed discussion of the results.

5.2 Sample preparation

Compact bone samples were prepared using the method described in Chapter 3. Fresh bone samples were macerated in a solution of water and Biozet detergent for a period of 5 days. The bones were then cleaned manually using a brush, knife and a scalpel. The samples that were manually cleaned were then cleaned in an ultrasonic cleaner. Cleaned samples were then cut using a diamond saw. The samples were prepared with two main objectives for this study.

- i) To investigate the effects of strain rates on the failure behavior of the cortical bone samples.
- ii) To investigate the effect of sample size on the failure behavior of the cortical bone samples.

The experimental plan was set up with samples sizes to be 30, 40, 50 and 60mm. The strain rate values were limited by the speed of data logging and the 3D strain measurement system. The strain rates were chosen to facilitate successful real-time strain measurement with sufficient displacement data and the number of images obtained from the tests. Transverse-section samples of 30, 40, 50 and 60 mm thickness were cut from the central femurs using a diamond saw machine at a low rotary speed. Alcohol was utilized as coolant during the cutting process. The samples were washed to remove any residual abrasives from the cutting. These samples were then visually inspected for any damage such as edge chipping and

uneven surfaces that could have occurred during the cutting process. Once it was ensured that the samples were cut as required and had the necessary parallel edges for compression testing, the samples were stored in a phosphor-buffered saline solution and kept refrigerated at -20°C until testing.

5.3 Compression testing

5.3.1 Mechanical apparatus

Compression testing of samples to investigate the effects of sample size and strain effects on cortical bone samples required the use of a Universal Testing Machine with control capabilities in the strain rate. The equipment used for the process was an INSTRON 5500 series. The INSTRON is a hydraulic Universal Testing Machine capable of recording load and displacement data at a frequency of up to 500Hz. The load cell used during the course of this investigation had a maximum capacity of a 100kN. The machine is controlled using Bluehill 2 software. The setup for the machine included compression plates of a diameter measuring 50 mm and the compression plates tooling. Compression tests were performed on the sample prepared at strain rates of 1.3, 2.3 and 3.3 mm/min.

5.3.2 Control system

The Bluehill 2 software was used to implement the control and data logging of compression during testing at 100Hz. The system was used because of the high repeatability and accuracy offered by the system. Bluehill 2 is the recommended

software for the control of the INSTRON 5500 series testing system. The design requirements for the system during the compression testing were:

- i) Control of the strain rate
- ii) Recording of the compressive force
- iii) Recording of the compressive displacement.

The system also caters to lower level requirements such as safety-limit switches and emergency switching operations.

5.3.3 Compression Test Procedure

The procedure for compression testing of bone samples can be described by the following steps.

1. The INSTRON testing system is switched on and the machine performs a self analysis test following prescribed checking tests.
2. The Bluehill control software is integrated with the testing system after the self analysis tests.
3. Test parameters such as strain rate, data collection and end of test are input into the control software.
4. Bone samples prepared are aligned on the compression plates such that the centre of the sample is aligned to the load cell
5. Once the test is ready to begin, the start button is pressed and the compression test was preformed.
6. Upon reaching the preset limits of the experiment, the control software stops the tests.

7. The cross head was then returned to its initial position and the sample removed.
8. Force and displacement data are saved.

For the experiments in this study, strain rates of 1.3, 2.3 and 3.3 mm/min were employed on sample lengths of 30, 40, 50 and 60 mm. Load displacement data was recorded for all the tests.

5.3.4 3D Real Time Strain Measurement

Real time strain measurement in cortical bone samples was achieved by the use of the ARAMIS 3D photogrammetry system. Photogrammetry is the technique of recording, measuring and interpreting the information of physical objects by the use of photographic images of the objects and patterns. This technique largely uses the principle of parallax for the recognition of the coordinates of the object. Two high speed, high resolution, digital CCD cameras record the images of the sample during the test and deformation was calculated from these images using an area-based matching algorithm. The two dimensional displacements recorded by each of the cameras are then correlated to a three dimensional measurement using intersection of the two dimensional measurements. The result is a three dimensional point distribution for each of the stages and the strain values are calculated from this point. This digital image provides a full-field contour of the sample and strain distribution throughout the test. The image sampling times used during these tests were maintained at *8ms*. Deformation and strain values ranging from 0.02% to 100% can be measured depending on the image quality. Figure 5.1 shows the experimental

set-up for compression testing on bones. During this study, the images focused on the sample between the two compression-plates of the INSTRON testing system.



Figure 5.1 Experimental set up for compression test

5.3.4.1 System specifications

The specifications for the ARAMIS system used while monitoring the compressions tests are as illustrated in Table 5.1. The type of lens used on the cameras and the position of the cameras largely defines the measuring volumes. There are a number of recommended measuring volumes and appropriate configurations supplied by the manufacturer, GOM, Germany. Due to the varying sample lengths in the study, measuring volumes of 40 x 30 x 30mm was used for surface strain measurements in 30 and 40 mm long samples and a measuring volume of 60 x 50 x 50 mm was used to characterize 50 and 60 mm long samples.

5.3.3: Specimen Preparation

Parameter	Specification
Measuring Volume	10x8x8 mm up to 1700x1360x1360 mm
Camera Resolution	1280x1024 pixels
Camera Chip	2/3", CCD
Maximum Frame Rate	24Hz
Maximum images	612
Shutter Time	0.1ms – 2s
Strain Range	0.05% - 100%
Strain accuracy	0.02%

Table 5.1: ARAMIS System specifications

Due to the high inter dependency of the frame rate, shutter speed and the aperture of the cameras, a number of tests were performed to achieve optimum balance between these factors. The lowest possible aperture was used in the cameras to achieve maximum depth in the volume and to accommodate the geometry of the bones. Trails made using two directional incandescent lights (500W) revealed a minimum shutter speed of $8ms$, which would allow successful image processing. The frame rate was calculated as 20Hz as maximum while using the shutter speed of $8ms$.

Compression tests were performed at 1.3, 2.3 and 3.3 mm/min. At strain rates higher than 3.3 mm/min, the number of images obtained was low and sudden failure behavior in bones was not well documented. This could also be attributed to the geometry of the bones.

5.3.5 Specimen Preparation

For the successful measurement of surface strain using the ARAMIS system, the surface structure of the samples is an important factor. The surface requirements for successful strain measurement are:

- i) low reflectivity
- ii) a high contrast stochastic pattern
- iii) sufficient lighting

A high contrast stochastic pattern is a histogram of equal proportions of black and white. This is essential for the allocation of coordinates on the surface of a specimen. The samples prepared were spray painted with a thin film of white paint. When the paint was sufficiently dry, the samples were coated with a spatter pattern of black on the surface to generate a high contrast stochastic pattern. Care was taken to keep the bones from drying by dropping approximately 5ml of phosphate buffer saline solution on the cut surfaces to maintain the material properties of the bone samples. The samples were tested immediately after the drying of the paint pattern. This process is sufficiently quick to prevent the bone samples from drying. Figure 5.2 shows a typical pattern applied to a bone sample prior to compression testing.



Figure 5.2: Stochastic pattern on bone sample

5.5 Results and Discussions

5.5.1 Load-Displacement Behavior

Results for the load displacement behavior will be presented at two sample sizes (30mm and 50mm) and two loading rates (1.3 mm/min and 3.3 mm/min) to elucidate the effect of sample size and loading rate. The results for the load displacement behavior for all the sample sizes and loading rates are given in Appendix A. Figure 5.3 shows the load displacement curve for a sample of length 30mm when tested at a strain rate of 1.3 mm/min. The load displacement curve is very smooth showing no signs of microcracking. There are no load drops in the curve to indicate any failure. The failure in the sample is catastrophic with no accumulated damage. The maximum load at failure in the sample is 12.135kN.

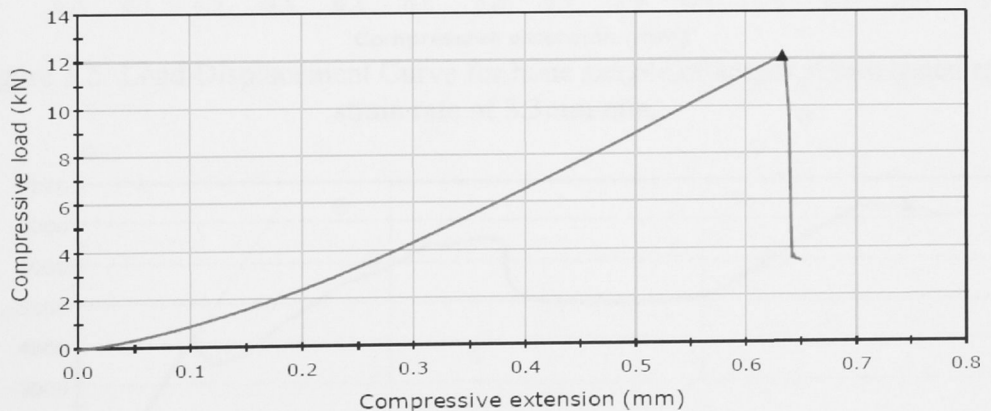


Figure 5.3: Load Displacement Curve for bone sample of length 30mm tested at a strain rate of 1.3mm/min.

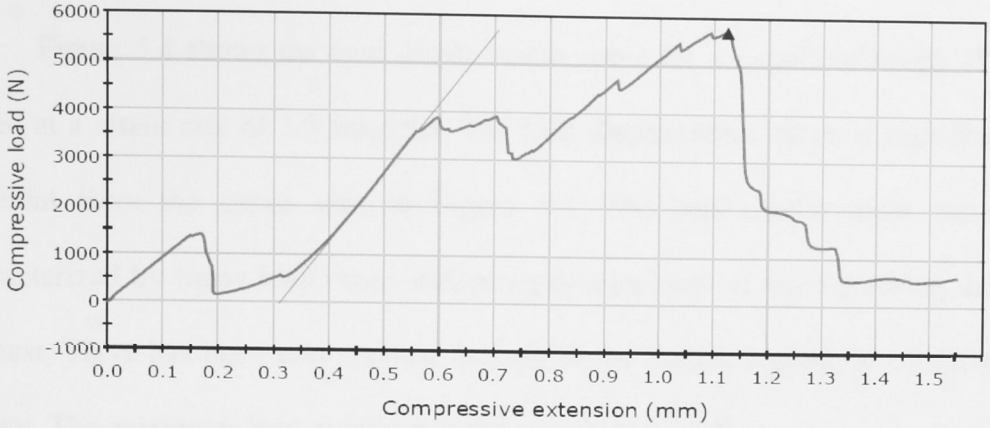


Figure 5.4: Load Displacement Curve for bone sample of length 50mm tested at a strain rate of 1.3mm/min.

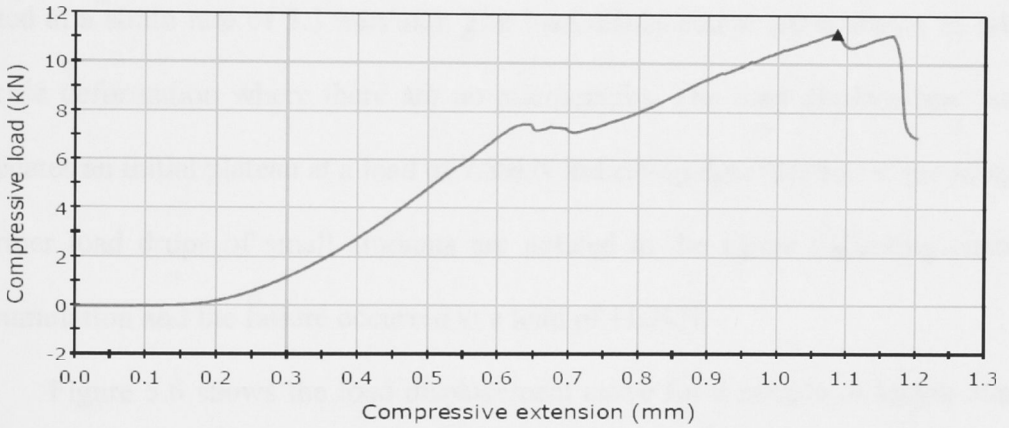


Figure 5.5: Load Displacement Curve for bone sample of length 30mm tested at a strain rate of 3.3mm/min.

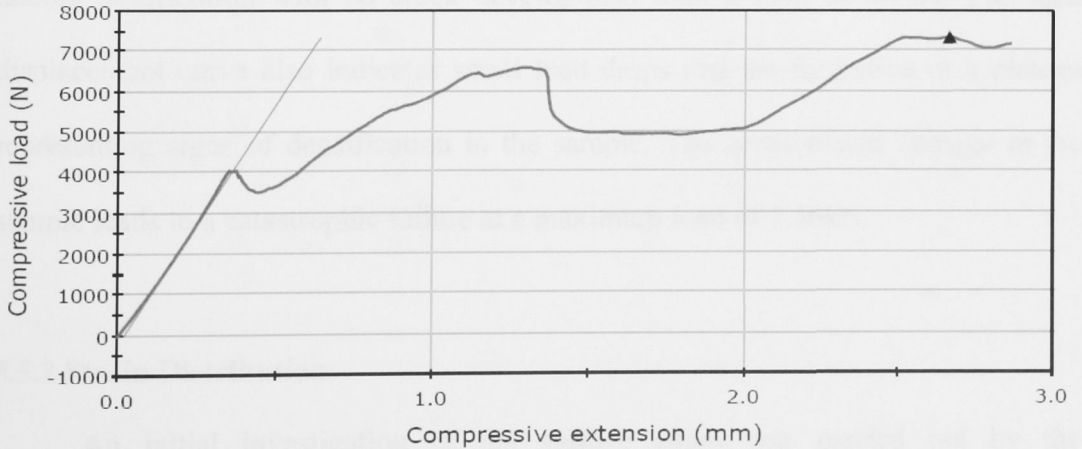


Figure 5.6: Load Displacement Curve for bone sample of length 50mm tested at a strain rate of 3.3mm/min.

Figure 5.4 shows the load displacement curve for a sample of length 50mm tested at a strain rate of 1.3 mm/min. The load displacement curve is significantly different from the curve seen in Figure 5.3. The load displacement curve is characterized by many load drops indicating development of microcracking during the test. There has been accumulated damage in the sample leading to catastrophic failure. The maximum load at failure in the sample is 5.72kN.

Figure 5.5 shows the load displacement curve for a sample of length 30mm tested at a strain rate of 3.3 mm/min. The load displacement curve shows an initial ductile deformation where there are no microcracks. The load displacement curve indicates an initial plateau at a load of 7.89kN indicating densification of the sample. Further load drops of small amounts are noticed in the figure indicating damage accumulation and the failure occurred at a load of 11.2kN.

Figure 5.6 shows the load displacement curve for a sample of length 50mm tested at a strain rate of 3.3 mm/min. The load displacement curve shows initial ductile deformation with no crack development until a load of 4.1kN. The load displacement curve also indicates small load drops and the formation of a plateau representing signs of densification in the sample. The accumulated damage in the sample leads to a catastrophic failure at a maximum load of 7.36kN.

5.5.2 Strain Distribution

An initial investigation of the surface strain was carried out by the observation of Von Mises strain distribution at failure in the samples. Figure 5.7

shows Von Mises strain distribution in a samples of lengths 30mm and 50mm tested at a strain rate of 1.3 mm/min. The strain distribution in the sample of length 30mm, seen in Figure 5.7(a), shows regions of higher strain distributed at different regions in the sample. The maximum strain recorded for the sample was 4.33%. The failure in the sample is catastrophic leading to the loss of the image in the optical measurement system. Figure 5.7(b) shows the Von Mises strain distribution in the sample of length 50mm tested at a strain rate of 1.3 mm/min. The strain in most regions of the sample was 2.16%. However the region near failure recorded a maximum strain value of 37.7%. This indicates a damage accumulation due to microcracking which ultimately formed a high strain concentration region. This region was the origin of a major crack that resulted in a catastrophic failure.

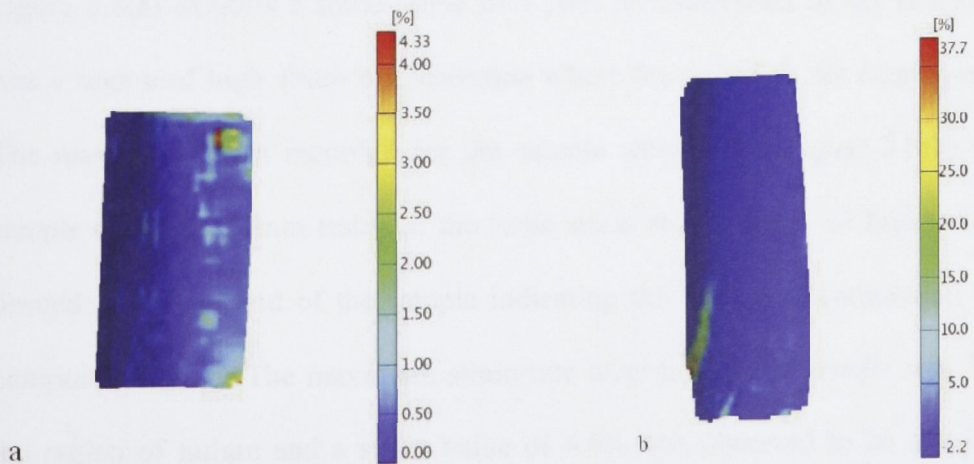


Figure 5.7: Von Mises strain distributions in bone samples, near failure, tested at 1.3mm/min. (a) Sample of length 30mm (b) Sample of length 50mm.

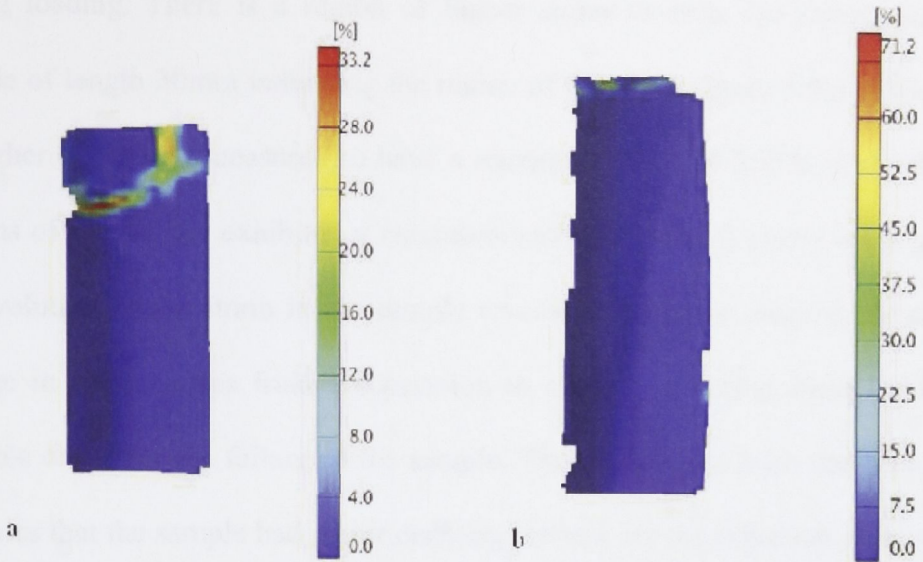


Figure 5.8: Von Mises strain distributions in bone samples, near failure, tested at 3.3mm/min. (a) Sample of length 30mm (b) Sample of length 50mm.

Figure 5.8 shows Von Mises strain distributions in samples of length 30 and 50mm loaded at a strain rate of 3.3 mm/min. The sample of length 30mm, as seen in Figure 5.8(a) exhibits a strain value of 3.16% for most parts of the sample. There was a region of high strain concentration where the failure in the sample occurred. The maximum strain recorded for the sample was 33.2%. Figure 5.8(b) shows a sample of length 50mm tested at the same strain rate. Regions of higher strain are limited to the top end of the sample indicating the damage accumulation near the compression plate. The maximum strain rate recorded for the sample was 71.2% at the region of failure and a strain value of 4.6% was observed to be distributed in most regions of the sample.

Figure 5.9 shows the distribution of major strain in bone samples of length 30 and 50mm tested at a strain rate of 1.3 mm/min. Major strain was used in these figures since it represents the dominating compressive strain experienced by samples

during loading. There is a region of higher strain towards the lower end of the sample of length 30mm indicating the region of failure in Figure 5.9(a). This region of higher strain was measured to have a maximum value of 3.85% while the most regions of the sample exhibited a maximum strain of 0.4%. A closer observation of the evolution of the strain in the sample revealed a behavior characterized by the change in strain values from compression to tension indicating shear failure as a possible cause for the failure of the sample. The observation from the micrographs indicates that the sample had major cracking through the cross section. Figure 5.9(b) shows the major strain distribution in a sample of length 50mm tested at a strain rate of 1.3 mm/min. The distribution contains a strain value of 1.9% in most parts of the sample and a region of high strain concentration showing the crack propagation during compression. The maximum value of major strain recorded was 18.9% for the sample.

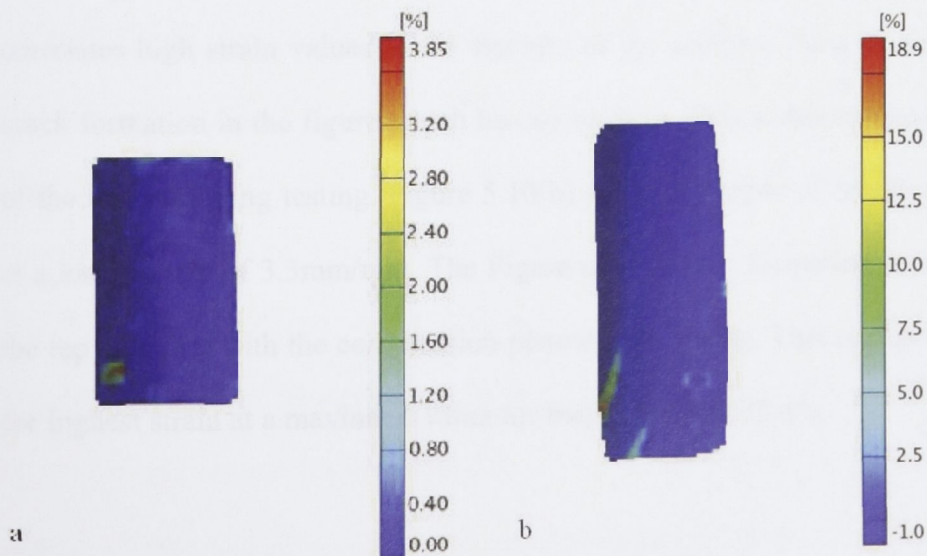


Figure 5.9: Major strain distribution in samples tested at a strain rate of 1.3 mm/min
(a) Sample of length 30mm (b) Sample of length 50mm.

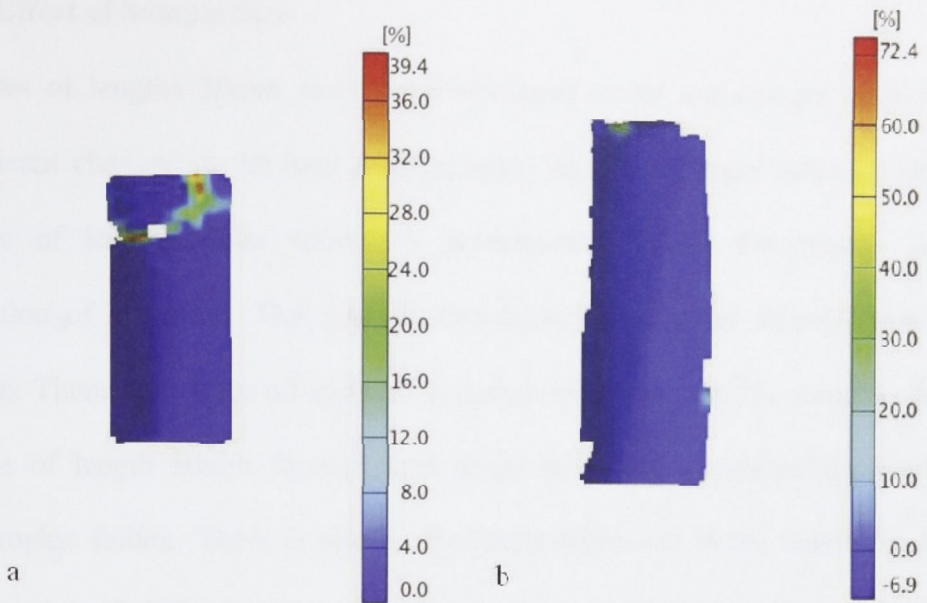


Figure 5.10: Major strain distribution in samples tested at a strain rate of 3.3 mm/min (a) Sample of length 30mm (b) Sample of length 50mm.

Figure 5.10 shows samples of length 30mm and 50mm tested at a loading rate of 3.3mm/min.. From Figure 5.10(a), it can be observed that the maximum value of major strain was 39.4% for the sample measuring 30mm in length. The figure correlates high strain values to the fracture of the sample. There is a region at the crack formation in the figure which has no reading. This is due to localized peeling of the sample during testing. Figure 5.10(b) shows a sample of length 50mm tested at a loading rate of 3.3mm/min. The Figure shows crack formation in the sample at the top interface with the compression plate during testing. This region has recorded the highest strain at a maximum value for major strain as 72.4%.

5.5.3 Effect of Sample Size

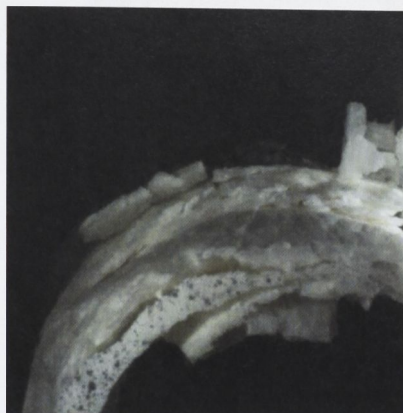
Samples of lengths 30mm and 50mm observed at the same strain rates showed significant changes in the load displacement curves and strain measurement. The sample of length 30mm showed a predominant ductile deformation and the formation of a plateau. This plateau formation indicates the densification in the sample. There have been no signs of accumulated damage in the sample while the sample of length 50mm showed load drops indicating microcracking leading to catastrophic failure. There is also a significant difference in the maximum load in the samples of different sizes. The failure load is observed to decrease with the increase in sample sizes. The densification of the samples of lower lengths explains the higher loads at failure in the samples. This densification is not observed in samples of lengths greater than 40mm and can be explained by the development of microcracks during the compression testing. The densification of samples was observed to prevent crack propagation. Samples of greater length were noticed to have a larger crack depth. From the strain distributions it can be observed that there is a significant change in the strain values measured in the samples of different sizes. An increase in the sample size has shown significant increase in the strain values measured. This increase in the strain values are a result of greater depth of the fracture in samples. A larger depth of fracture allows for greater deformation on the surface of the sample leading to higher strain values which are concentrated in the region of fracture. Although significant changes have been observed in the load displacement curves and the strain distribution, samples of different lengths have shown similar failure with shear failure as the predominant mechanism.

5.5.4 Effect of Strain rate

From the observations of experimental results of both load displacement behavior and the strain distribution, it can be noticed that there are significant changes in the failure behavior of bone samples in compression when tested at different strain rates. The load displacement data indicates development of microcracking in the samples of greater length when tested at higher strain rates. The strain distributions in the samples tested at different rates also indicate a significant change in the magnitude of the maximum strain values at the region of failure. The maximum strain values recorded a significant increase with the increase in strain rate in all samples. There has also been a significant change in the failure behavior in the samples. Densification was noticed to be higher in the sample of lower lengths while the samples of larger length showed greater damage accumulation when tested at higher rates such as 3.3 mm/min. Samples tested at lower strain rates show crack propagation along the long axis of the bone samples. This is seen in Figure 5.9. Directional cracking was observed in samples tested at higher strain rates. The cracking was observed to propagate in a direction perpendicular to the loading direction. In samples of smaller lengths the crack was initiated in the direction of loading and was further propagated in a direction perpendicular to the loading axis. This is observed in Figures 5.10 (a) and (b).

5.6 Microscopic observations

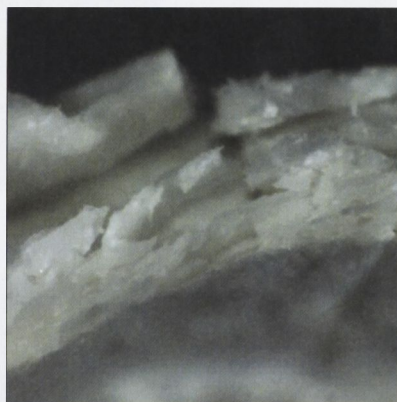
It is the complex microstructure that determines the failure of bone materials. Fracture in the bone samples has been observed using an optical microscope (WILD, 1-32x, USA) with variable magnification. Figure 5.11(a) shows the fracture region in a 30mm length sample, which was tested at a rate of 1.3 mm/min, at 8x magnification. The figure reveals the layered nature of the bone after failure. There are a number of layers which have been formed and it is from these regions that fracture has evolved to the surface. Figure 5.11(b) shows a sample of length 30mm tested at a strain rate of 2.3 mm/min. There are noticeable lesser number of layers formed between the outer and inner surfaces. Figure 5.11(c) shows a sample of length 30 mm tested at a high loading rate of 3.3 mm/min. This sample shows cracking in just one layer. The secondary cracking perpendicular to the layer formation is a result of localized interaction with the loading plate.



(a)



(b)

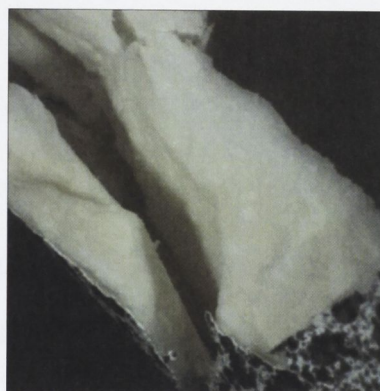


(c)

Figure 5.11 Magnified images of bone fracture. (a) Fracture in 30mm long sample tested at 1.3 mm/min (b) Fracture in 30mm long sample tested at 2.3 mm/min (c) Fracture in 30mm long sample tested at 3.3 mm/min



(a)



(b)



(c)

Figure 5.12. Fracture in the cross section of bone (a) Cracking in sample loaded at 1.3 mm/min. (b) Cracking in sample loaded at 2.3 mm/min (c) Cracking in sample loaded at 3.3 mm/min

The Figures 5.12(a), 5.12(b) and 5.12(c) show three samples of 50mm length that were subjected to loads of 1.3, 2.3 and 3.3 mm/min respectively. The Figures show differences in the cracking of bones during the tests at different strain rates. The sample shows fracture to have occurred in many layers between the outer and inner diameters. The depth of the cracks are also larger compared to those in 30mm long samples. The figure shows the region of the fracture to be between the outer and inner surfaces, apart from the fracture on the longitudinal surface of the bone. This fracture is initiated in a similar manner as seen in Figure 5.12(a). The difference being that fracture has occurred splitting the inner and outer surfaces to just two layers. The fracture region is similar to that seen in Figure 5.12(b) where the fracture was initiated predominantly between the outer and inner surfaces in just a single layer, with the crack showing a large depth.

Closer observations of Figures 5.11 and 5.12 reveal similar cracking mechanisms in similar loading conditions. A noticeable difference was the depth of the cracking. Samples of length show a lower depth in all the cracked regions while the cracking observed in the 50mm long samples of Figure 5.12 show a greater depth of the cracked regions. Greater depths of fracture are observed to be the factor for lower peak loads at failure and greater strain values measured at the region of failure.

5.7 Summary of Compression testing of compact bone

- Significant effect of sample size and loading rate has been observed in compact bones tested in compression
- Increase in sample size showed a decrease in the maximum load at failure
- Samples with higher lengths exhibited microcracking while samples with lower sizes showed no damage accumulation.
- Failure was observed to be catastrophic at lower strain rates with no built up damage
- Increase in loading rate increased failure strain values recorded in the samples for all sizes
- Time dependant behavior was observed in samples tested at different loading rates
- Geometry of the samples was observed to have an effect on the failure evolution
- Orientation of fractures was found to be different in the samples tested at higher strain rate

3 Point Bend Testing of Compact Bones

6.1 Introduction

Bones sustain damage mainly due to cyclic loading and impact. 3 Point bending tests on bones provides details of the mechanical behavior of bone in both compression and tension. The failure during this type of testing also provides key information important for treating bone fractures. The bone material is known to have same modulus in both compression and tension but fractures at lower stresses in tension than in compression. This asymmetrical behavior has been noticed by bone researchers and has been attributed to the microstructure of the bones [59]. The haversian canals and mineralization in the bone material is known to influence the bones more in compression than in tension during bending tests [76]. The experimental results of the literature provide an integral view to the effects of rate of applied loading but fail to elucidate the role of loading rates on localized processes leading to the failure in bone samples. This study aims to provide a better understanding of localized processes which lead to failure by the investigation of strain measurements and strain evolution in bone material subjected to 3 point bending.

6.2 Experimental Procedure

6.2.1 Sample preparation

Compact bone samples were prepared by the method using Biozet detergent, described in Chapter 3 earlier in this thesis. The samples were prepared with two main objectives for the study.

- i) To investigate the effects of the strain rates on the failure behavior of the cortical bone samples in bending
- ii) To study the evolution of strain in bones during bending and correlate the strain evolution with the failure of bones.

The samples needed relatively lesser preparation compared to the compression samples as they did not require any edge preparation. The samples that were cleaned were stored in a phosphor buffered saline solution and kept refrigerated at -20°C until testing.

6.3 Point Bend testing

6.3.1 Mechanical apparatus

The INSTRON 5500 series universal testing machine was used for the 3 point bend testing of bone samples. A 100kN load cell and optical extension encoder were used to record the test data. The machine is controlled using the Bluehill 2 software. The setup for the machine included 3 point bend test rigs which has a changeable span between the bottom 2 supports. 3 point bend tests were performed on the sample prepared at strain rates of 1.3, 2.3 and 3.3 mm/min. The experimental set up for the tests are shown in Figure 6.1.

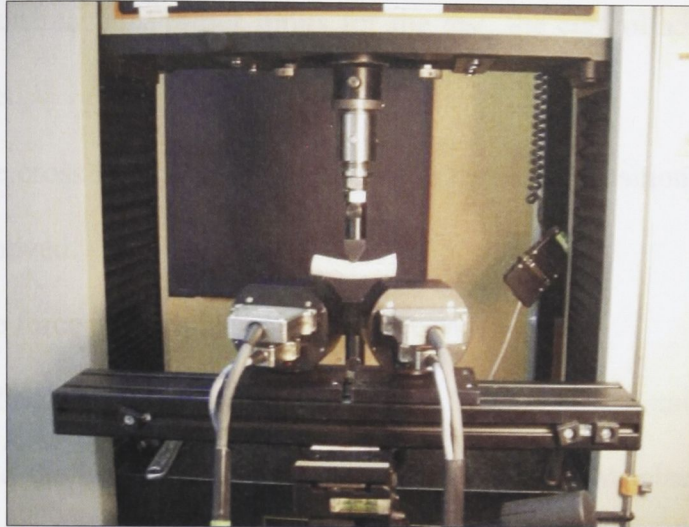


Figure 6.1: Experimental set up for 3 point bend testing of bones.

6.3.2 3 Point Bend Test Procedure

The procedure for the 3 point bend testing of the bone samples can be described by the following steps.

1. The INSTRON testing system is switched on and the machine performs a self analysis test following prescribed checking tests.
2. The Bluehill control software is integrated with the testing system after the self analysis tests.
3. Test parameters such as the strain rate, data collection and end of test are input into the control software.
4. Bone samples prepared are aligned on the bending rig such that the edges are equidistant from the bending points.
5. Once the test is ready to begin, the start button was pressed and the 3 point bend test was preformed.

6. Upon reaching preset limits for the test, the control software stops the tests.
7. The cross head was then returned to the initial position and the sample removed.
8. The force and displacement data are saved.

The loading rates for the compression test have been maintained for bending keeping in mind the limitations of the equipment. The load displacement data was recorded for all the tests. The geometric details of the test are as below:

Parameter	Measurement
Sample Length	75 mm
Sample diameter (effective)	3.8 mm
Distance between loading pins	30 mm
Test span	60 mm
Diameter of loading pin	5 mm

6.3.3 3D Real Time Strain Measurement

Strain measurements were conducted using the ARAMIS 3D photogrammetry system. The lens used for this study was of 17 mm focal length. The cameras were calibrated to a measuring volume of 100 x 80 mm. The cameras were configured for conducting the measurements at a frame rate of 20Hz with the shutter speed being 8ms. A stochastic pattern was sprayed on the samples to achieve a high contrast

image with low reflectivity. The pattern is similar to those applied during the compression tests. The samples were ready for the tests when the paint pattern was dry.

6.4 Results and Discussions

6.4.1 Load Displacement Behavior

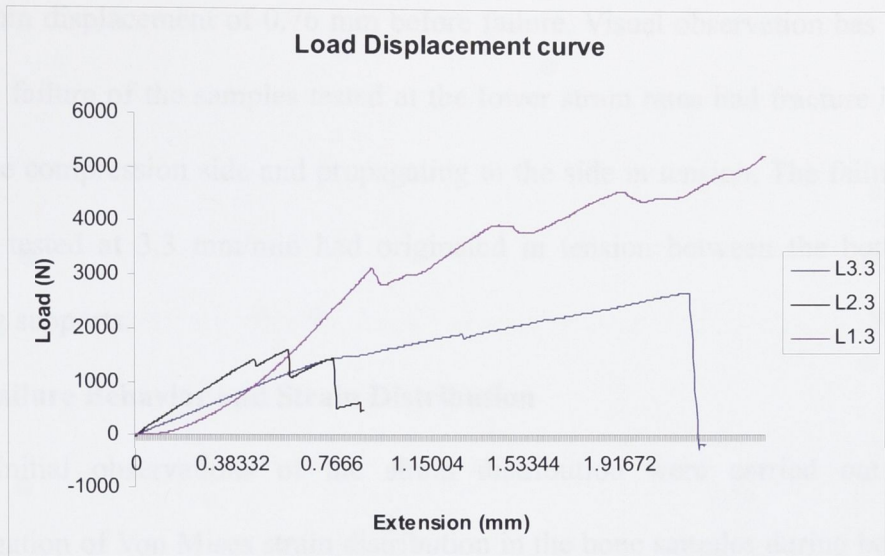


Figure 6.2: Load Displacement curves for samples tested at different loading rates.

Loading rates have been observed to have a significant effect on the failure behavior of bones during 3 point bending. Figure 6.2 shows the load displacement curves for three samples tested at strain rates of 1.3 mm/min, 2.3 mm/min and 3.3 mm/min. The peak load at failure was observed to reduce with increase in the loading rates during testing. This behavior is similar to the behavior observed during the compression testing of bones in Chapter 5. The peak load recorded for sample tested at 1.3 mm/min showed a peak load of 5.2kN. The peak load for the samples tested at 2.3 mm/min and 3.3 mm/min were 2.41kN and 1.6kN respectively. The displacement in the samples was observed to be significantly different at different loading rates. The Load Displacement curves for the three strain rates show that the samples tested in lower strain rates, such as 1.3 m/min and 2.3 mm/min, had a much higher value for displacement before failure compared to sample tested at a higher strain rate, such as 3.3 mm/min. Samples tested at 1.3mm/min and 2.3 mm/min had

displacements of 3mm and 2.25 mm while the sample tested at 3.3 mm/min had a maximum displacement of 0.76 mm before failure. Visual observation has revealed that the failure of the samples tested at the lower strain rates had fracture initiating from the compression side and propagating to the side in tension. The failure in the sample tested at 3.3 mm/min had originated in tension between the bottom two bending supports.

6.4.2 Failure Behavior and Strain Distribution

Initial observations of the strain distribution were carried out by the investigation of Von Mises strain distribution in the bone samples during bend tests. Figure 6.3 shows the Von Mises strain distribution in bone before the failure for a sample tested at a strain rate of 1.3 mm/min. The strain distribution showed most part of the samples to experience a strain of 0.2%. The maximum Von Mises strain recorded for the sample was 2.12%.

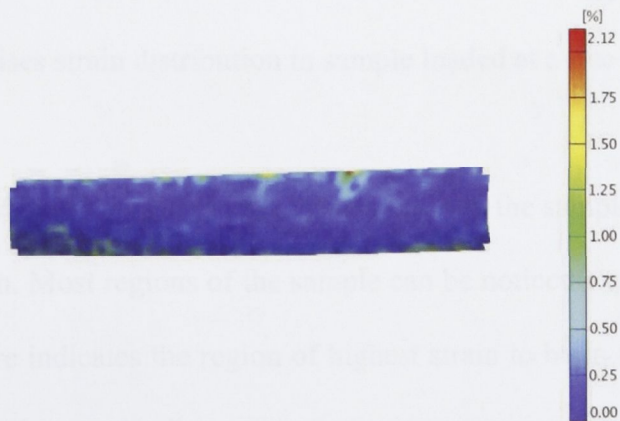


Figure 6.3: Von Mises strain distribution in sample loaded at a rate of 1.3 mm/min.

Figure 6.4 shows Von Mises strain distribution in bone sample tested at a strain rate of 2.3 mm/min. The strain distribution illustrates that high strain values

were concentrated in two primary regions; near the contact point of the top loading roller and one of the bottom loading rollers of the test rig. The strain values in these regions are higher compared to most regions of the sample. The maximum strain recorded for the sample at failure was 10.6% while most regions of the sample exhibited a strain value of 1.2%. Major cracking occurred between the regions of high strain concentration with the fracture initiating from the region in compression and propagating to the region in tension.

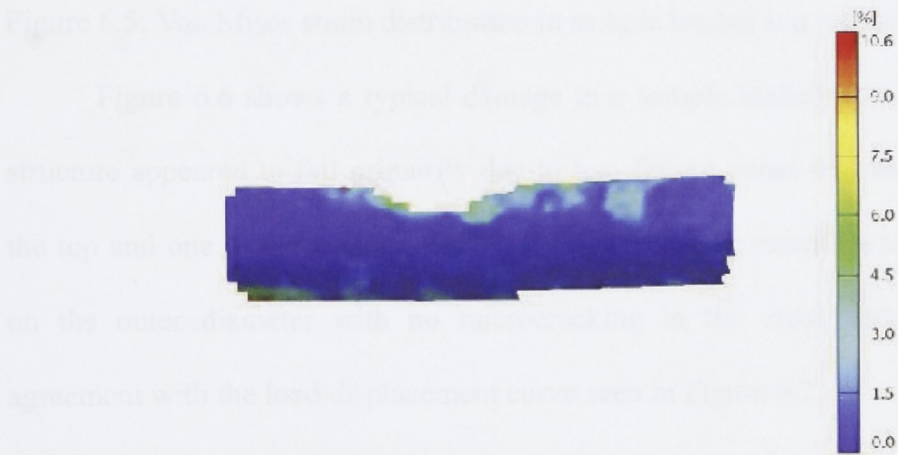


Figure 6.4: Von Mises strain distribution in sample loaded at a rate of 2.3 mm/min.

Figure 6.5 shows Von Mises strain distribution in the sample tested at a strain rate of 3.3 mm/min. Most regions of the sample can be noticed experiencing a strain of 0.8%. The figure indicates the region of highest strain to be in the bottom part of the sample near the bottom loading roller. A maximum strain of 7.46% was recorded for the sample.

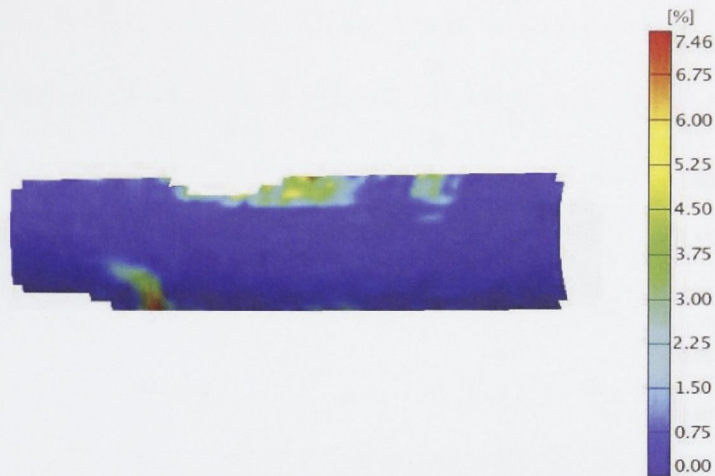


Figure 6.5: Von Mises strain distribution in sample loaded at a rate of 3.3 mm/min.

Figure 6.6 shows a typical damage in a sample loaded at 1.3 mm/min. The structure appeared to fail primarily due to two failure zones that were located near the top and one of the bottom rollers. The failure in the sample was predominantly on the outer diameter with no microcracking in the cross section. This is in agreement with the load displacement curve seen in Figure 6.2.



Figure 6.6: Typical damage in sample loaded at 1.3 mm/min

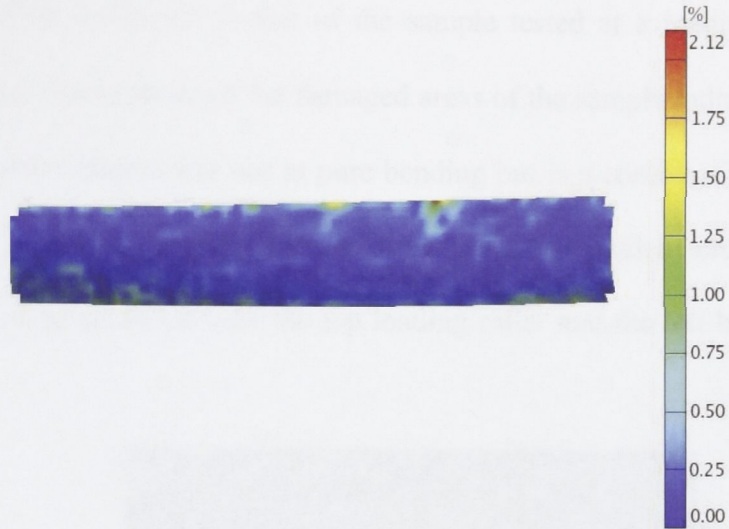


Figure 6.7: Major strain distribution in sample loaded at 1.3 mm/min during the test

Figure 6.7 shows the major strain distribution in the sample near failure when tested at a loading rate of 1.3 mm/min. In most parts of the sample, the strain distribution was observed to be 0.2%. A region with a high magnitude of strain can be observed near the top loading roller on the compression side of the sample. This region formed the origin of the failure. There is a region of increased strain also observable near the bottom roller. The maximum major strain recorded for the sample at these regions was 2.12%. The two regions form the end points in the fracture evolution. The fracture of the sample occurred between these points during the testing

Figure 6.8 shows typical damage in bone samples loaded at a strain rate of 2.3 mm/min. The failure in the sample is similar to the sample tested at 2.3 mm/min. major strain distribution in the sample during the evolution of failure is seen in Figure 6.9. in most part of the sample the strain value was determined to be 0.6% and a maximum strain value at the region of failure was 9.1%. This pattern of

fracture evolution is similar to that of the sample tested at a loading rate of 1.3 mm/min. Visual observations of the damaged areas of the sample indicate the failure is neither in pure compression nor in pure bending but is a combination of the two. The fractures of the samples tested at the lower rates were sudden across the regions of high strain concentrations near the top loading roller and the left bottom loading roller.

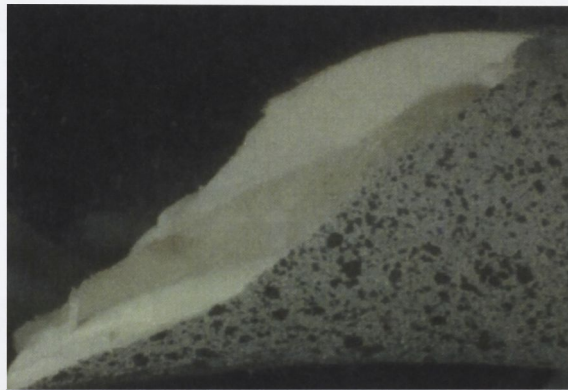


Figure 6.8 : Typical damage in sample loaded at 2.3 mm/min

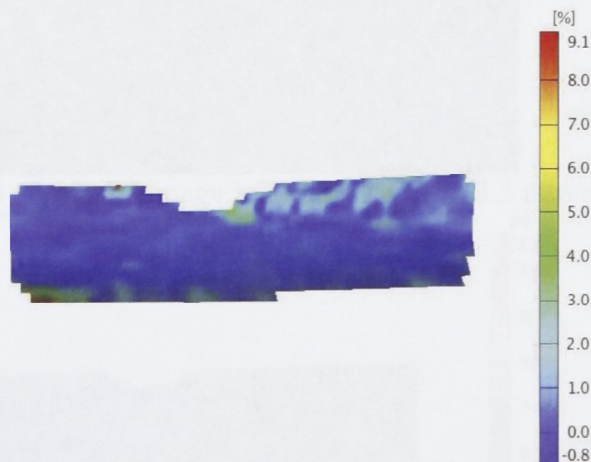


Figure 6.9: Major strain distribution in sample loaded at 2.3 mm/min during the test

A notably different failure mode was observed in the sample tested at the strain rate of 3.3 mm/min. Figure 6.10 illustrates a typical failure in a sample loaded at 3.3 mm/min. The crack development as seen in the sample is between the bottom

loading rollers and the crack runs along the long axis of the bone. Figure 6.11 shows strain distribution in the sample during failure. There is a region of higher strain in the bottom part of the sample. It is also observed that there is a smaller region of increased strain value at the point of contact with the top loading roller of the 3 point bend test. The difference in the sample loaded at 3.3 mm/min when compared to Figure 6.7 is that there are regions of higher strain concentration near the loading rollers but not at the regions of tension experienced by the sample. The fracture of the sample was sudden and has been unable to view using the ARAMIS strain measurement system

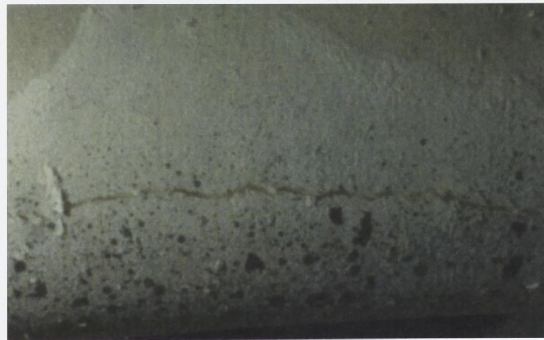


Figure 6.10: Typical damage in sample tested at 3.3 mm/min.

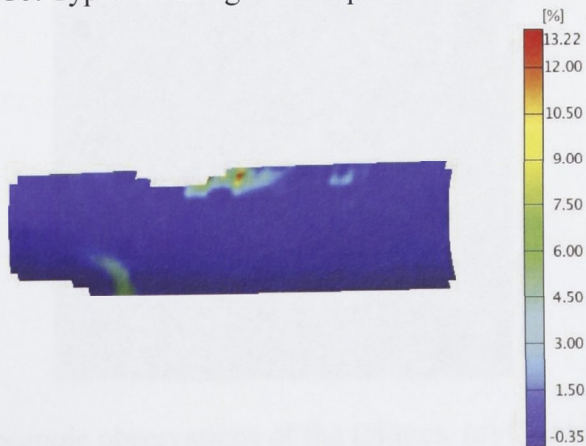


Figure 6.11: Major strain distribution in sample loaded at 3.3 mm/min during the test

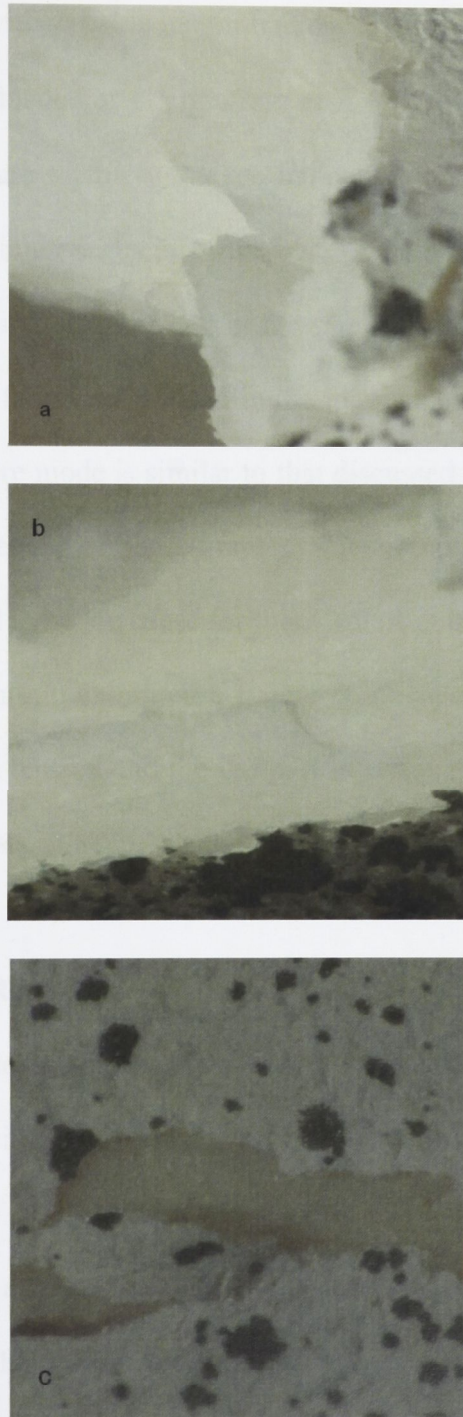


Figure 6.12: Microscopic observations of the failures. (a) Cracking in the sample loaded at 1.3 mm/min, 32x, (b) Cracking in the sample loaded at 2.3 mm/min, 32x, (c) Cracking in the sample loaded at 3.3 mm/min, 32x.

Microscopic observations were performed using an optical microscope (WILD, 1-32x, USA) with variable magnification. Figure 6.12(a) shows a part of the fracture in the sample loaded at 1.3 mm/min at 3200% of magnification. It can be observed that the fracture region is uneven indicating there may be some shearing between the outer and inner surfaces of the bone. This phenomenon is also noticed in the sample as seen in Figure 6.12(b) in the sample loaded at a strain rate of 2.3 mm/min. This form of failure is initiated in the top part of the bone which is under compression. This failure mode is similar to that discussed in Chapter 5 which deals with the compression testing of bone samples. Microstructure and mineralization in the bones was observed to be the cause for this form of failure. The sample loaded at a strain rate of 3.3 mm/min exhibited a failure dominated by tension. The bottom part of the sample is in tension and the top part in compression when the sample is subjected to bending tests.

6.5.3 Effect of Strain Rates

The load displacement curves for samples tested at the three strain rates also indicate different behavior of the samples. The sample tested at a rate of 1.3 mm/min shows an initial ductile curve with no damage up to a load of 3 kN. There is a load drop at 3kN indicating a failure or a crack formation. The maximum load at failure in the sample was 5.2 kN with some load drops. These load drops elucidate crack propagation. These fractures in the sample could be the possible result of the geometry of the sample. In a sample tested at 2.3 mm/min there is a more ductile deformation with no accumulated damage. The failure is sudden and catastrophic.

The sample loaded at rate of 3.3 mm/min shows a different load displacement curve with a maximum load of just 1.6kN with many load drops. There is a continuous accumulation of damage in the sample and at little deformation. This indicates a more brittle mechanical failure. The strain measurement system provides a value for the strain throughout the image. The average measured strain is an indication of the strain distribution throughout the sample. The average strain in the area was found to change with the changes in strain. The sample loaded at a strain rate of 1.3 mm/min had an average strain of 1.19% and the average strain in the sample loaded at a rate of 2.3 mm/min was 3%. The value of the average strain in the sample loaded at 3.3 mm/min was however 9%. The maximum values of strain in the samples loaded at 1.3, 2.3 and 3.3 mm/min were 6%, 9.45% and 13.42% respectively. There has been an increase in the strain values recorded with the increase in loading rates. This study has shown from the experimental results the importance of the loading rates in the failure behaviour of bone material.

6.6. Summary of 3 Point bend testing of compact bones

- Significant effect of loading rates was observed in samples tested
- Higher strain rates lowered the maximum load at failure in samples tested
- Higher strain rates were characterized by reduced displacement in the direction of loading
- Failure was observed to be a combination of compression and tension at lower strain rates

- Failure was observed to be in tension when loading rate of 3.3 mm/min was used

- Strain values were observed to increase with increase in loading rate
- Different failure modes were identified at different loading rates

References

[1] Meyer, R. L., 1970, "The Mechanical Properties of Bone: A Review of the Literature," *Journal of Biomechanics*, Vol. 3, pp. 399-408.

[2] Weiner, S., Wagner, I.D., 1990, "The Structure and Mechanical Function of Bones: Anisotropic Properties," *Annual Review of Biomedical Engineering*, Vol. 20, pp. 271-294.

[3] Cudde, A., Michalski, M., Lajunen, S., Chiriac, R., Gnanou, C., Gualardi, A., Laine, M., Burchard, M., Rindfleisch, S., Kowalek, J., 1992, "Orientation of Mineral Crystals by Collagen Fibrils During *in vivo* Bone Engineering: An X-ray Diffraction Imaging Study," *Biotechnology and Bioengineering*, Vol. 42, pp. 641-647.

[4] Bradley, D.A., Madsen, P., Ellis, E.B., Green, T.M., Anderson, J., Smith, R., Arkell, K., Colridge, D.B., Wainwright, C.P., 2001, "The Mineralization of Bone and Cartilage: *in vivo* Diffraction and Crystallographic Fluorescence Microscopy," *Nuclear Instruments and Methods in Physics Research B*, Vol. 263, pp. 1-6.

[5] Peters, P., Schwanz, K., Epple, M., 2007, "The Structure of Bone Studied with synchrotron X-ray Diffraction, X-ray Absorption Spectroscopy, and Raman Analysis," *Techniques in Chemistry*, Vol. 101, pp. 131-138.

[6] Rakita, E., Cherdron, F., Mautner, P.H.A., Tabet, Z., Weindl, A., 2001, "Studies of Crystal Orientation and Calcium Distribution in Trabecular Bone," *Nuclear Instruments and Methods in Physics Research B*, Vol. 240, pp. 16-24.

[7] Speller, B., Paul, N., Tzaphanidis, M., Bonfield, W., 2005, "MicroCT Analysis of Calcium Phosphate-rich Sites of Degenerating Bone Sites," *Nuclear Instruments and Methods in Physics Research B*, Vol. 348, pp. 278-273.

References:

- [1] Meyers, M.A., Chen, P-Y., Lin, A.Y.M, Seki, Y., 2008, *Biological Materials: Structure and Mechanical Properties*, Progress in Material Science, Vol. 53, p: 1-206.
- [2] Weiner, S., Wagner, H.D., 1998, *The Material Bone: Structure- Mechanical Function Relations*, Annual Reviews Material Sciences, Vol. 28, p: 271- 298.
- [3] Cedola, A., Mastrogiacomo, M., Lagomarsino, S., Cancedda, R., Giannini, C., Gualardi, A., Ladisa, M., Burghammer, M., Rusticelli, F., Komlev, V., 2007, *Orientation of Mineral Crystals by Collagen Fibres During In Vivo Bone Engineering: An X- ray Diffraction Imaging Study*, Spectrochimica Acta Part B, Vol. 62, p: 642- 647.
- [4] Bradley, D.A., Muthuvelu, P., Ellis, R.E., Green, E.M., Attenburrow, D., Barrett, R., Arkill, K., Colridge, D.B., Winlove, C.P., 2007, *Characterization of Mineralization of Bone and Cartilage: x- ray Diffraction and Ca and Sr K_{α} X- ray Fluorescence Microscopy*, Nuclear Instruments and Methods in Physics Research B, Vol. 263, p: 1- 6.
- [5] Peters, F., Schwarz, K., Epple, M., 2007, *The Structure of Bone Studied with synchrotron X- ray Diffraction, X- ray Absorption Spectroscopy and Thermal Analysis*, Thermochemica Acta, Vol. 361, p: 131- 138.
- [6] Rokita, E., Chevallier, P., Mustaers, P.H.A., Tabor, Z., Wróbel, A., 2005, *Studies of Crystal Orientation and Calcium Distribution in Trabecular Bone*, Nuclear Instruments and Methods in Physics Research B, Vol. 240, p: 69- 74.
- [7] Speller, R., Pani, S., Tzaphilidou, M., Horrocks, J., 2005, *MicroCT Analysis of Calcium/ Phosphorus ratio Maps at Different Bone Sites*, Nuclear Instruments and Methods in Physics Research B, Vol. 548, p: 269- 273.

[8] Gonchar, A.M., Klomogrov, U.P., Gladkikh, E.A., Shuvaeva, O.V., Beisel, N.F., Kolosova, N.G, 2005, *The Estimation of The Possibilities of Synchrotron Radiation X- ray Fluorescent Analysis and Atomic Spectrometry for The Bone's Elemental Composition Determination*, Nuclear Instruments and Methods in Physics Research A, Vol. 543, p: 271- 273.

[9] Tzaphilidou, M., Berillis, P., Matthopoulos, D., 2005, *Bone Calcium Phosphorus Detection by Auger Electron Spectroscopy*, Micron, Vol. 36, p: 706- 709.

[10] Cooper, D.M.L., Thomas, D.L., Clement, J.G., Turinsky, A.L., Sensen, C.W., Hallgrimsson, B., 2007, *Age- Dependant Change in 3D Structure of Cortical Porosity at The Human Femoral Midshaft*, Bone, Vol. 40, p: 957- 965.

[11] Chaffai, S., Peyrin, F., Nuzzo, S., Porcher, R., Berger, G., Laugier, P., 2002, *Ultrasonic Characterization of Human Cancellous Bone Using Transmission and Backscatter Measurements: Relationships to Density and Microstructure*, Bone, Vol. 30, Iss. 1, p: 229-237.

[12] Bouxsein, M.L., 2003, *Bone Quality: Where Do We Go From Here?*, Osteoporos International, Vol. 14, Suppl. 5, p: 118- 127.

[13] Yuan, H., Chen, N., Xiaoying, L., Zheng, B., Cui, W., Song, X., 2005, *Natural Hydroxyapatite/ Chitosan Composite for Bone Substitute Materials*, Proceedings of the 2005 IEEE Engineering in Medicine and Biology 27th Annual Conference.

[14] Athanasiou K.A., Zhu C-F., Lanctot, D.R., Agrawal, C.M., Wang, X., 2003, *Fundamentals of Biomechanics in Tissue Engineering of Bone*, Tissue Engineering, Vol. 6, p: 361– 381.

[15] Riches, P.E., Everitt, N.M., Heggie, A.R., McNally, D.S., 1997, *Microhardness Anisotropy of Lamellar Bone*, J Biomech, Vol. 30, p: 1059– 1061.

- [16] Mahoney, E., Holt, A., Swain, M., Kilpatrick, N., 2000, *The Hardness and Modulus of Elasticity of Primary Molar Teeth: An Ultra-Micro-Indentation Study*. J Dent, Vol. 28, p: 589– 594.
- [17] Riches, P.E., Everitt, N.M., McNally, D.S., 2000, *Knoop Microhardness Anisotropy of the Ovine Radius*. J Biomech, Vol. 33, p: 1551– 1557.
- [18] Ramrakhiani, M., Pal, D., Murty, T., 1979, *Micro-indentation Hardness Studies on Human Bones*. Acta Anatomica, Vol. 103, p: 358– 362.
- [19] Meredith, N., Sherriff, M., Setchell, D. J., Swanson. S. A. V., 1996, *Measurement of Microhardness and Young's Modulus of Human Enamel and Dentine Using an Indentation Technique*, Archives Oral Biology, Vol. 41, p: 539– 545.
- [20] Xu, H.H.K., Smith, D.T., Jahanmir, S., Romberg, E., Kelly, J.R., Thompson, V.P., Rekow, E.D., 1998, *Indentation Damage and Mechanical Properties of Human Enamel and Dentin*, J Dent Res., Vol. 77, p: 472– 480.
- [21] Zioupos, P., Kaffy, C., Currey, J.D., 2006, *Tissue Heterogeneity, Composite Architecture and Fractal Dimension Effects in the Fracture of Ageing Human Bone*, International Journal of Fracture, Vol. 139, p: 407- 424.
- [22] Currey, J.D., 2003, *Role of Collagen and Other Organics in the Mechanical Properties of Bone*, Osteoporos International, Vol. 14, Suppl. 5, p: 29- 36.
- [23] Yi, W., Heo, M., Lee, S., Choi, S., Huh, K., Lee, S., 2007, *Direct Measurement of Trabecular Bone Anisotropy Using Directional Fractal Dimension and Principal Axes of Inertia*, OOOOE, Vol. 104, Iss. 1, p: 110- 116.
- [24] Evans, A.G., Charles, E.A., 1976, JAM, Vol. 59, p: 371-xxx.

- [25] Yang, Q.D., Cox, B.N., Nalla, R.K., Ritchie, R.O., 2006, *Fracture Length Scales in Human Cortical Bone: The Necessity of Non- Linear Fracture Models*, *Biomaterials*, Vol. 27, p: 2095- 2113.
- [26] Iyo, T., Maki, Y. Sasaki, N., Nakata, M., 2004, *Anisotropic Viscoelastic Properties of Cortical Bone*, *Journal of Biomechanics*, Vol. 37, p: 1433- 1437.
- [27] Guedes, R.M., Simões, J.A., Morias, J.L., 2006, *Viscoelastic Behaviour and Failure of Bovine Cancellous Bone under Constant Strain Rate*, *Journal of Biomechanics*, Vol. 39, p: 49- 60.
- [28] George, W.T., Vashishth, D., 2005, *Damage Mechanisms and Failure Modes of Cortical Bone under Components of Physiological Loading*, *Journal of Orthopaedic Research*, Vol. 23, p: 1047- 1053.
- [29] Flachsmann, R., Broom, N.D., Hardy, A.E, 2001, *Deformation and Rapture of the Articular Surface under Dynamic and Static Compression*, *Journal of Orthopaedic Research*, Vol. 19, p: 1131- 1139.
- [30] Tekyeh- Marouf, B., Bagheri, R., 2007, *Fracture Behavior of Multi- Layered composites under Impact Loading*, *Material Science and Engineering A*, Vol. 448, p: 20- 24.
- [31] Ferriera, F., Vaz, M.A., Simões, J.A., 2006, *Mechanical Properties of Bovine Cortical Bone at High Strain Rate*, *Materials Characterization*, Vol. 57, p: 71- 79.
- [32] Beck, T. 2003, *Measuring the Structural Strength of Bones with Dual- Energy X-ray Absorptiometry: Principles, technical Limitations and Future Possibilities*, *Osteoporos International*, Vol. 14, Suppl. 5, p: 81- 88.
- [33] Majumder, S.R., Mazumdar, S., 2007, *Mechanical breakdown of Trabecular Bone: Dependence on Microstructure*, *Physica A*, Vol. 377, p: 559- 564.

[34] Katz, J.L., 1971, *Journal of Biomechanics*, Vol. 4, p: 455- 473.

[35] Johnson, W.M, Rapoff, A.J., 2007, *Microindentation in Bone: Hardness Variation with Five Independent Variables*, *Journal of Material Sciences: Materials in Medicine*, Vol. 18, p: 591- 597.

[36] Nalla, R.K., Kinney, J.H., Ritchie, R.O., 2003, *Mechanistic fracture criteria for the failure of human cortical bone*, *Nature Materials*, Vol. 2, p: 164– 168.

[37] Tai, K., Dao, M., Suresh, S., Palazoglu, A., Ortiz, C., 2007, *Nanoscale heterogeneity promotes energy dissipation in bone*, *Nature Materials*, Vol. 6, p: 454– 462.

[38] Gao, H., Ji, B., Jäger, I.L., Arzt, E., Fratzl, P., 2003, *Materials Become Insensitive to Flaws at Nanoscale: Lessons from Nature*, *PNAS*, Vol. 100, p: 5597– 5600.

[39] Peterlik, H., Roschger, P., Klaushifer, K., Fratzl, P., 2006, *From Brittle to Ductile Fracture of Bone*, *Nature Mater*, Vol. 5, p: 52– 55.

[40] Fantner, G.E., Hassenkam, T., Kindt, J.H., Weaver, J.C., Birkedal, H., Pechenik, L., Cutron, J.A., Cidade, G.A.G., Stucky, G.D., Morse, D.E., Hansma, P.K., 2005, *Sacrificial Bonds and Hidden Length Dissipate Energy as Mineralized Fibrils Separate During Bone Fracture*. *Nature Mater*, Vol. 4, p: 612– 616.

[41] Upta, H.S., Stachewicz, U., Wagermaier, W., Roschger, P., Wagner, H.D., Fratzl, P., 2006, *Mechanical Modulation at the Lamellar Level in Osteonal Bone*. *J Mater Res*, Vol. 21, p: 1913– 1921.

- [42] Hassenkam, T., Fantner, G.E., Cutroni, J.A., Weaver, J.C., Morse, D.E., Hansma, P.K., 2004, *High-Resolution AFM Imaging of Intact and Fractured Trabecular Bone*. *Journal of Structural Biology*, Vol. 35, p: 4– 10.
- [43] Augat, P., Schorlemmer, S., 2006, *The Role of Cortical Bone and its Microstructure in Bone Strength*. *Age Ageing*, Vol. 35, Suppl. 2, p: 27– 31.
- [44] Taylor, D., Hazenberg, J.G., Lee, T.C., 2007, *Living with Cracks: Damage and Repair in Human Bone*. *Nature Mater*, Vol. 6, p: 263– 268.
- [45] An, Y.H., Draughn, R.A., 2000, *Mechanical Testing of Bone and the Bone-Implant Interface*. Florida: CRC Press.
- [46] Amanat, N., He, L.H., Swain, M.V., Little, D.G., 2007, *The Effect of Zoledronic Acid on the Intrinsic Material Properties of Healing Bone: An Indentation Study*. *Med Eng Phys*.
- [47] Barak, M.M., Sharir, A. Shahar, R., 2008, *Optical Metrology Methods for Mechanical Testing of Whole Bones*, *The Veterinary Journal*.
- [48] Ebacher, V., Tang, C., McKay, H., Oxland, T. R., Guy, P., Wang, R., 2007, *Strain redistribution and cracking behavior of human bone during bending*. *Bone*, Vol. 40, p: 1265 – 1275.
- [49] Yan, J., Mecholsky Jr, J.J., Clifton, K.B., 2007, *How Tough is Bone? Application of Elastic- Plastic Fracture Mechanics to Bone*, *Bone*, Vol. 40, p: 479- 484.

[50] Lucksanasombool, P., Higgs, W.A.J., Higgs, R.J.E.D., Swain, M.V., 2001, *Fracture Toughness of Bovine Bone: Influence of Orientation and Storage Media*, *Biomaterials*, Vol. 22, p: 3127- 3132.

[51] Ladd, A.J.C., Kinney, J.H., Haupt, D.L., Goldstein, S.A., 1998, *Finite Element Modeling of Trabecular Bone: Comparison with mechanical Testing and Determination of Tissue Modulus*, *Journal of Orthopaedic Research*, Vol. 16, p: 622-628.

[52] Evans, G.P., Behiri, J.C., Currey, D.J., Bonfield, W., 1990, *Microhardness and Young's Modulus in Cortical Bone Exhibiting a Wide Range of Mineral Volume Fractions, and in a Bone Analogue*, *J Mater Sci: Mater Med*, Vol. 1, p: 38– 43.

[53] Nalla, R.K., Stolken, J.S., Kinney, J.H., Ritchie, R.O., 2005, *Fracture in Human Cortical Bone: Local Fracture Criteria and Toughening Mechanisms*, *Journal of Biomechanics*, Vol. 38, p: 1517- 1525.

[54] Follet, H., Peyrin, F., Vidal- Salle, E., Bonnassie, A., Rumelhart, C., Meunier, P.J., 2007, *Intrinsic Mechanical Properties of Trabecular Calcaneus Determined by Finite- Element Models Using 3D Synchrotron Microtomography*, *Journal of Biomechanics*, Vol. 40, p: 2174- 2183.

[55] Bevill, G., Eswaran, S.K., Gupta, A., Papadopoulos, P., Keaveny, T.M., 2006, *Influence of Bone Volume Fraction and Architecture on Computed Large-Deformation Failure Mechanisms in Human Trabecular Bone*, *Bone*, Vol. 39, p: 1218- 1225.

[56] Beaupied, H., Lespessailles, E., Benhamou, C., 2007, *Evaluation of Macrostructural Bone Biomechanics*, *Joint Bone Spine*, Vol. 74, p: 233- 239.

[57] Kasra, M., Grynbas, M.D., *On Shear Properties of Trabecular Bone under Torsional Loading: Effects of Bone Marrow and Strain Rate*, *Journal of Biomechanics*.

[58] Fleck, C., Eifler, D., 2007, *Influence of the Loading Rate on the Cyclic Deformation Behaviour and the Damage Accumulation of the Cortical Bone Specimens Under Three- Point Bending*, *Advanced Engineering Materials*, Vol. 9, Iss. 12, p: 1069- 1076.

[59] Robling, A.G., Castillo, A.B., Turner, C.H., 2006, *Biomechanical and Molecular Regulation of Bone Remodeling*. *Annu Rev Biomed Eng.*, Vol. 8, p: 455– 498

[60] Athanasiou K.A., Zhu C-F., Lanctot, D.R., Agrawal, C.M., Wang, X., 2003, *Fundamentals of Biomechanics in Tissue Engineering of Bone*, *Tissue Engineering*, Vol. 6, p: 361– 381.

[61] Malik, C.L., Gibeling, J.C., Martin, R.B., Stover, S.M. *Journal of Biomechanics*, Vol. 36, p: 194.

[62] Liebschner, M.A.K., 2004, *Biomechanical Consideration of Animal Models Used in Tissue Engineering of Bone*. *Biomater.*, Vol. 25, p: 1697– 1714.

[63] Buehler, M.J., 2007, *Nano and Micromechanical Properties of Hierarchical Biological Materials and Tissues*. *J Mater Sci.*, Vol. 42, p: 8765– 8770

[64] Roy, M.E., Rho, J-Y., Tsui, T.Y., Evans, N.D., Pharr, G.M., 1999, *Mechanical and Morphological Variation of the Human Lumbar Vertical Cortical and Trabecular Bone*. *J Biomed Mater Res.*, Vol. 44, p: 191– 197

[65] Currey, J.D., 2002, *Bones: Structure and Mechanics*. New Jersey: Princeton University Press.

[66] Fantner, G.E., Hassenkam, T., Kindt, J.H., Weaver, J.C., Birkedal, H., Pechenik, L., Cutron, J.A., Cidade, G.A.G., Stucky, G.D., Morse, D.E., Hansma, P.K., 2005,

Sacrificial Bonds and Hidden Length Dissipate Energy as Mineralized Fibrils Separate During Bone Fracture. Nature Mater, Vol. 4, p: 612– 616.

[67] Olszta, M.J., Cheng, X., Jee, S.S., Kumar, R., Kim, Y., Kaufman, M.J., Douglas, E.P., Gower, L.B., 2007, *Bone Structure and Formation: A New Perspective*, Material Sciences and Engineering R.

[68] Hoc, T., Henry, L., Verdier, M., Aubry, D., Sedel, L., Meunier, A., 2006, *Effect of Microstructure on the Mechanical Properties of Haversian Cortical Bone.* Bone Vol. 38, p: 466– 474.

[69] Giannini, M., Soares, C.J., de Carvalho, R.M., 2004, *Ultimate Tensile Strength of Tooth Structures,* Dent Mater, Vol. 20, p: 322– 329.

[70] Everitt, N.M., Rajah, S., McNally, D.S., 2006, *Bone Recovery Following Indentation,* J Bone Joint Surgery - British Volume, Vol. 88B, p: 398.

[71] Fan, Z., Rho, J-Y., 2003, *Effects of viscoelasticity and Time-dependent Plasticity on Nano-indentation Measurements of Human Cortical Bone,* J Biomed Mater Res, Vol. 67A, p: 208– 214.

[72] Nalla, R.K., Kruzic, J.J., Kinney, J.H., Ritchie, R.O., 2005, *Mechanistic Aspects of Fracture and R-curve Behavior in Human Cortical Bone.* Biomater Vol. 26, p: 217– 231.

[73] Quinn, J.B., Quinn, G.D., 1997, *Indentation of Brittle of Ceramics: A Fresh Approach*, J Mater Sci, Vol. 32, p: 4331– 4346.

[74] Rho, J-Y., Tsui, T.Y., Pharr, G.M., 1997, *Elastic Properties of Human Cortical and Trabecular Lamellar Bone Measured by Nanoindentation*, Biomater, Vol. 18, p: 1325– 1330.

[75] Zysset, P.K., Guo, X.E., Hoffler, C.E., Moore, K.E., Goldstein, S.A., 1999, *Elastic Modulus and Hardness of Cortical and Trabecular Bone Lamellae Measured by Nanoindentation in the Human Femur*. Journal of Biomech, Vol. 32, p: 1005– 1012.

[76] Yan, J., Mecholsky Jr, J.J., Clifton, K.B., 2007, *How Tough is Bone? Application of Elastic- Plastic Fracture Mechanics to Bone*, Bone, Vol. 40, p: 479- 484.

Appendix A

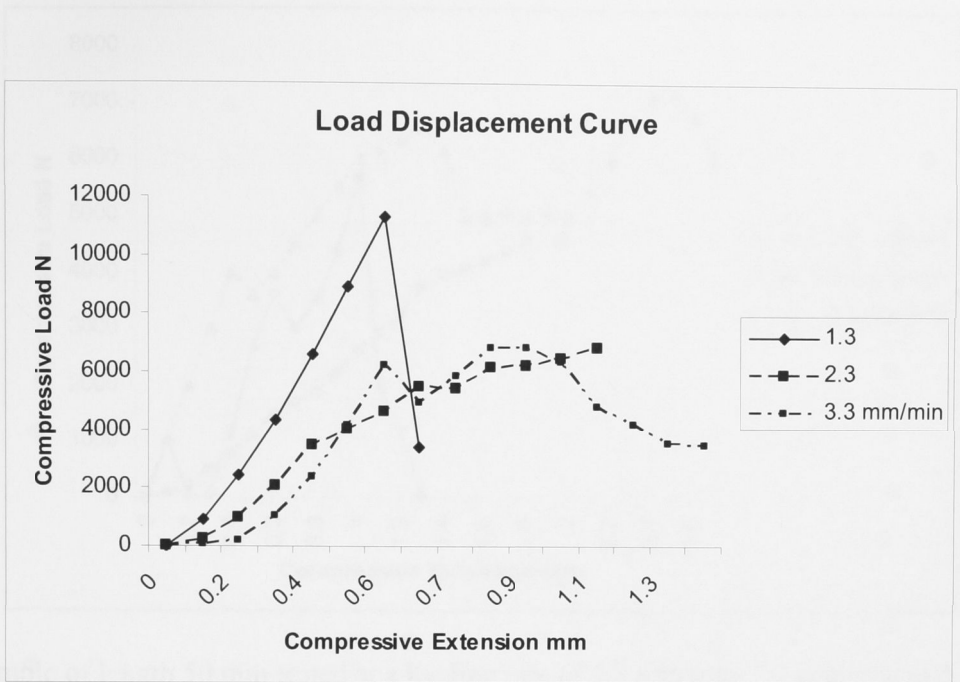
LOAD DISPLACEMENT BEHAVIOUR

Load displacement curves for all the all bone samples tested in compression are presented here.



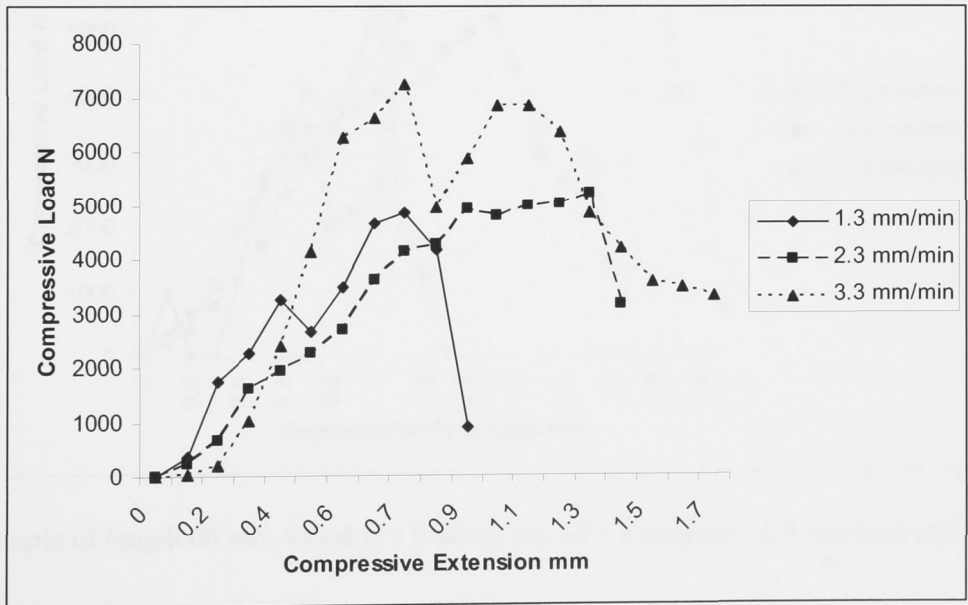
Sample of length 40 mm tested at a loading rate of 1 mm/min. 2.5 mm diameter, 3.5 mm diameter, 3.5 mm diameter.

FIGURE 1



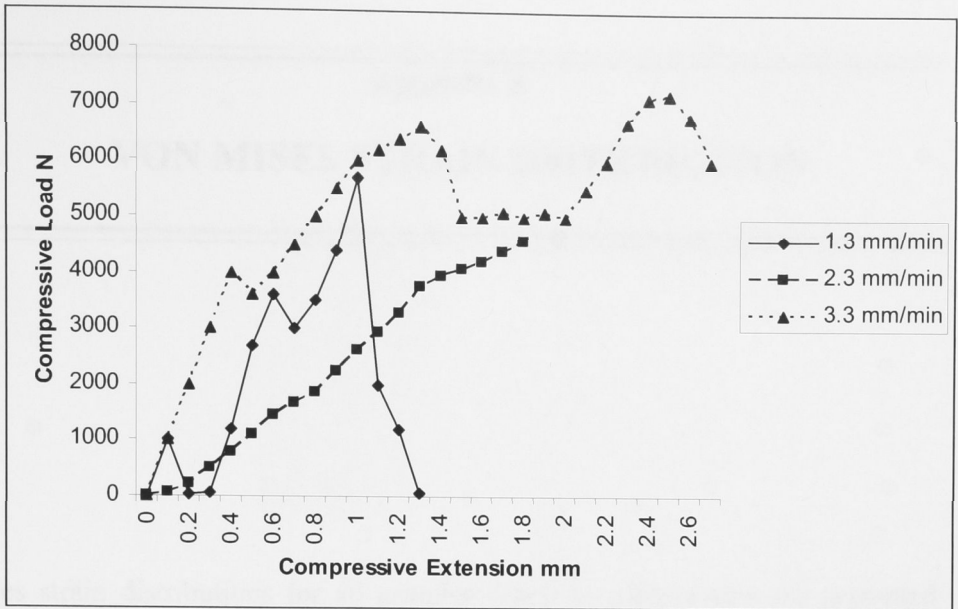
Sample of length 30 mm tested at a loading rate of 1.3 mm/min, 2.3 mm/min and 3.3

mm/min

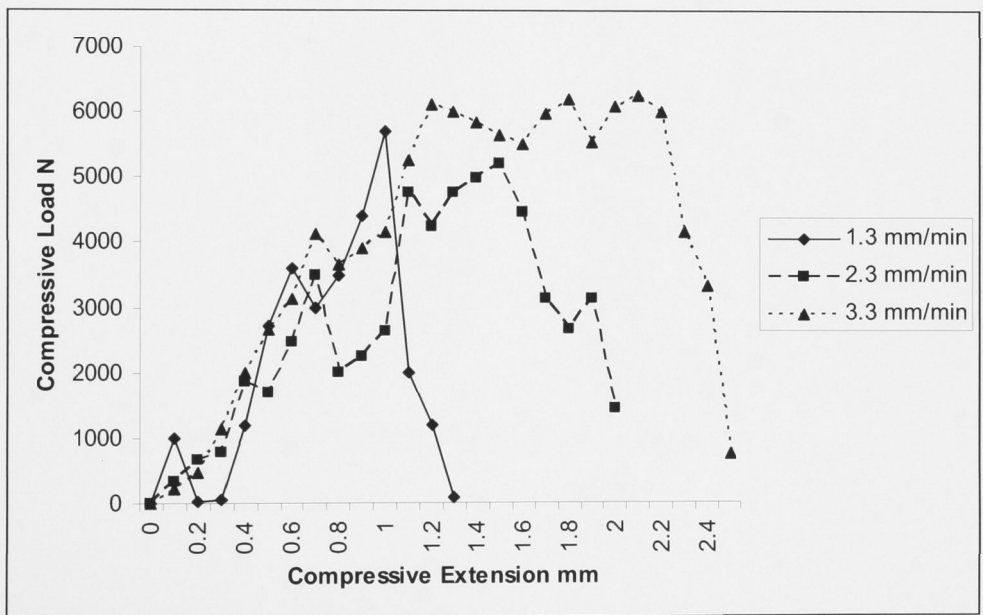


Sample of length 40 mm tested at a loading rate of 1.3 mm/min, 2.3 mm/min and 3.3

mm/min



Sample of length 50 mm tested at a loading rate of 1.3 mm/min, 2.3 mm/min and 3.3 mm/min



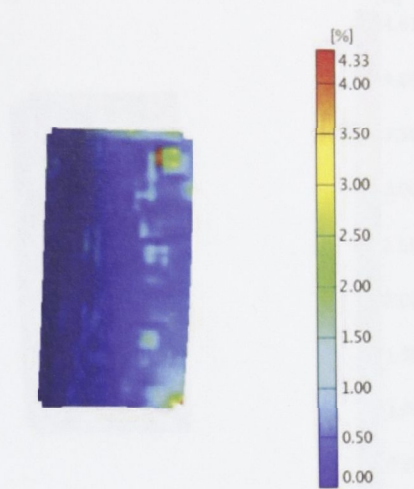
Sample of length 60 mm tested at a loading rate of 1.3 mm/min, 2.3 mm/min and 3.3 mm/min

Appendix B

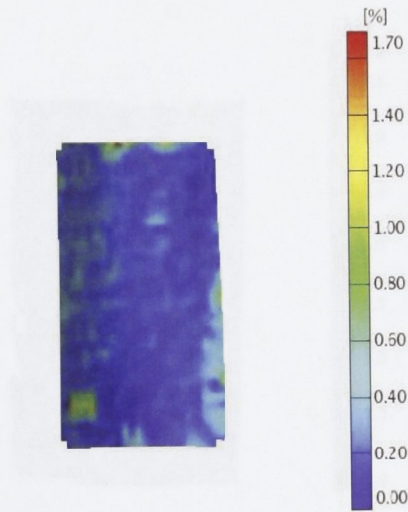
VON MISES STRAIN DISTRIBUTION

Von Mises strain distributions for all samples tested in compression are presented here. The strain distributions are closer to failure in the samples.

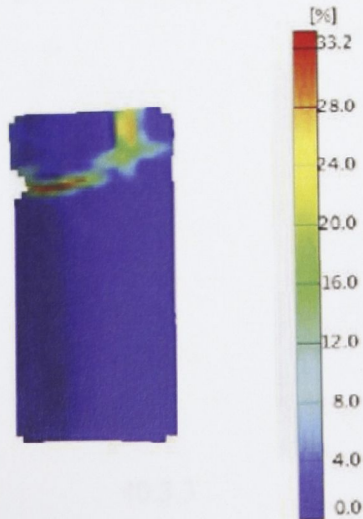
Samples of length 30 mm tested at the different loading rates are presented here.



Sample loaded at a rate of 1.3 mm/min

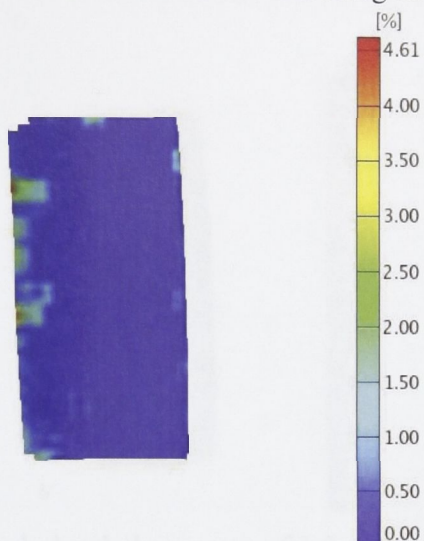


Sample loaded at a rate of 2.3 mm/min

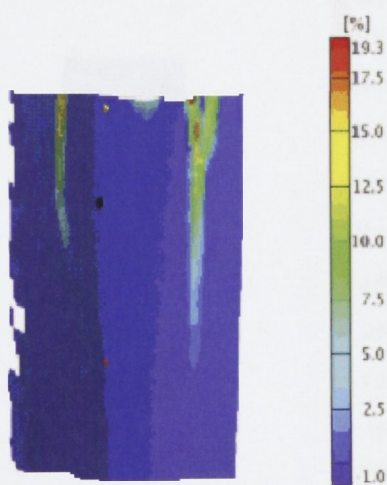


Sample loaded at a rate of 3.3 mm/min

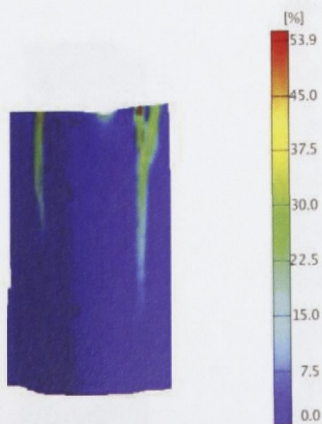
Samples of length 40 mm tested at the different loading rates are presented here.



Sample loaded at a rate of 1.3 mm/min



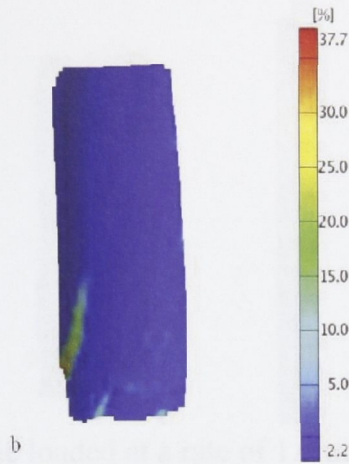
Sample loaded at a rate of 2.3 mm/min



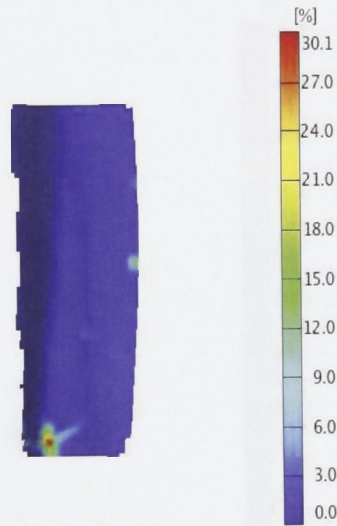
40.3.3

Sample loaded at a rate of 3.3 mm/min

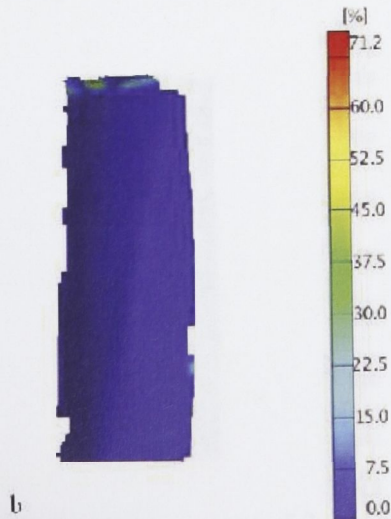
Samples of length 50 mm tested at the different loading rates are presented here.



Sample loaded at a rate of 1.3 mm/min

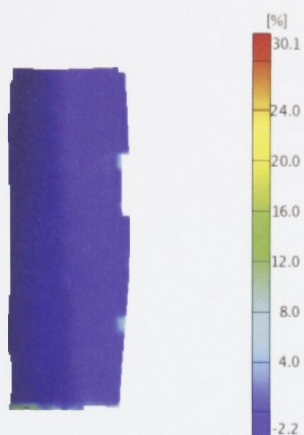


Sample loaded at a rate of 2.3 mm/min

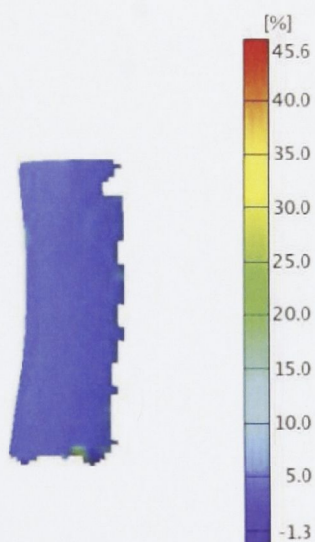


Sample loaded at a rate of 3.3 mm/min

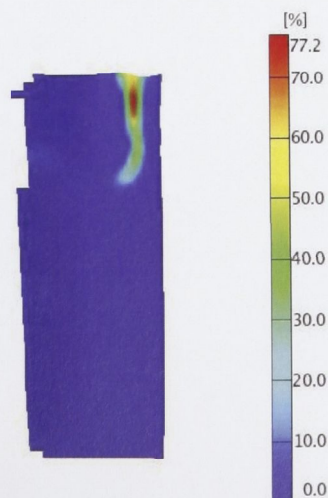
Samples of length 60 mm tested at the different loading rates are presented here.



Sample loaded at a rate of 1.3 mm/min



Sample loaded at a rate of 2.3 mm/min



Sample loaded at a rate of 3.3 mm/min